

Figure 8.16. Device B full bandwidth pulse shape.

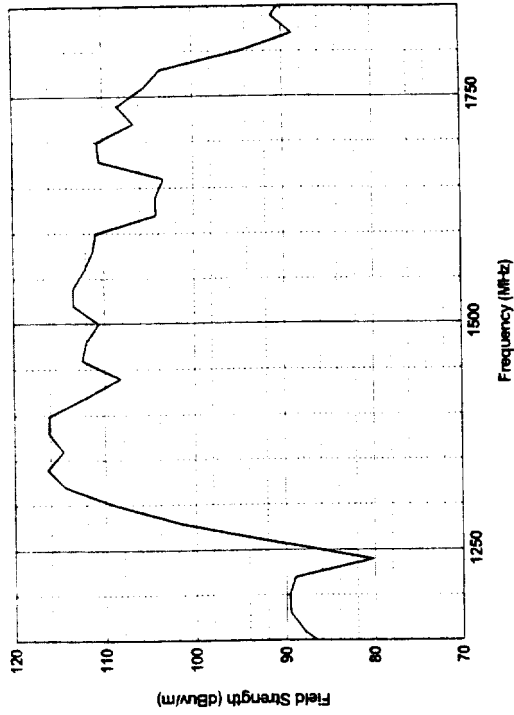


Figure 8.17. Device B, radiated peak field strength at 1 m, $\Delta f = 20$ MHz.

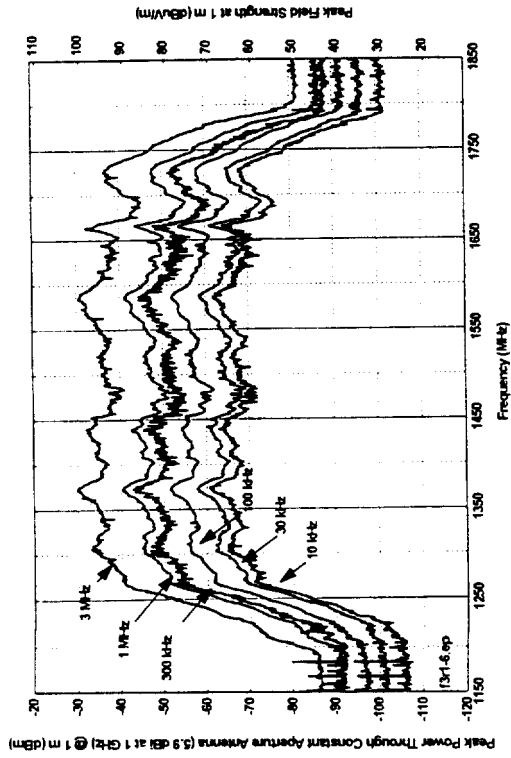


Figure 8.18. Device B, spectra as a function of bandwidth, 16-kb/s voice mode.

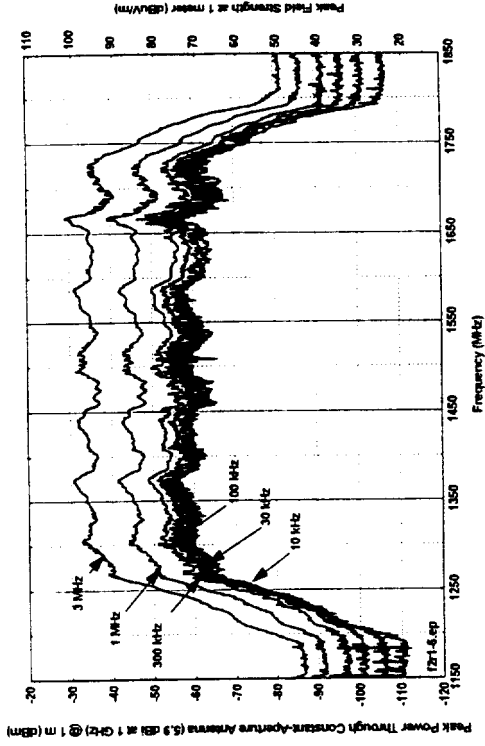


Figure 8-19. Device B, spectra as a function of bandwidth, 128-kb/s voice mode.

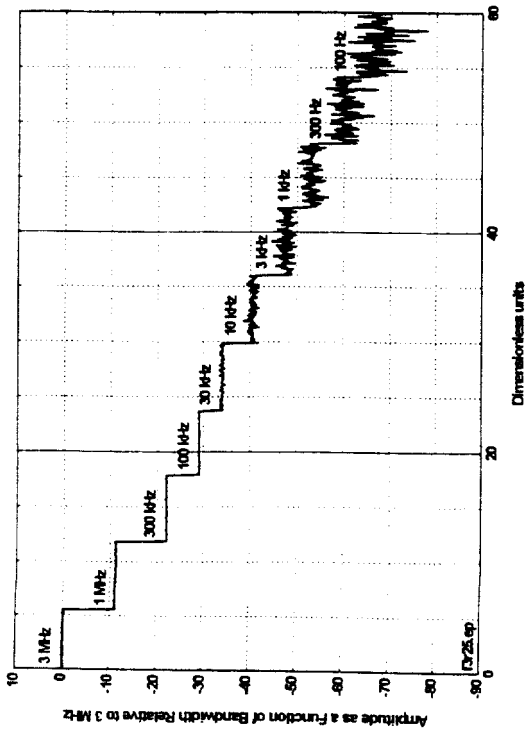


Figure 8.20. Device B, 16-kb/s voice mode, bandwidth progression staircase.

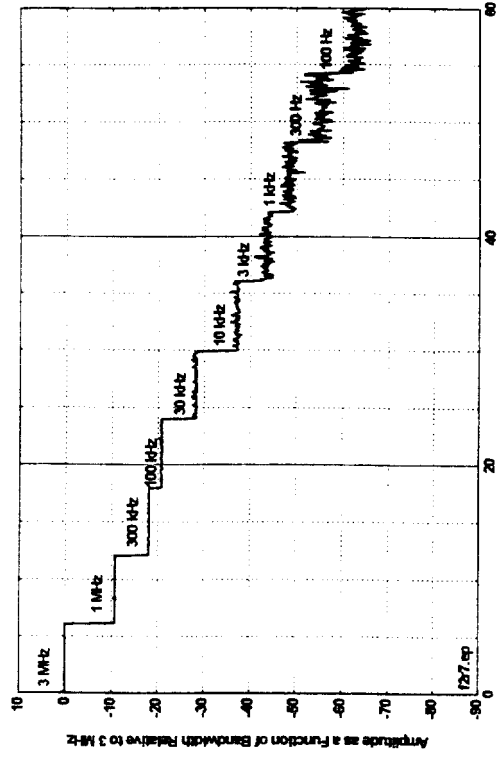


Figure 8.21. Device B, 128-kb/s voice mode, bandwidth progression staircase.

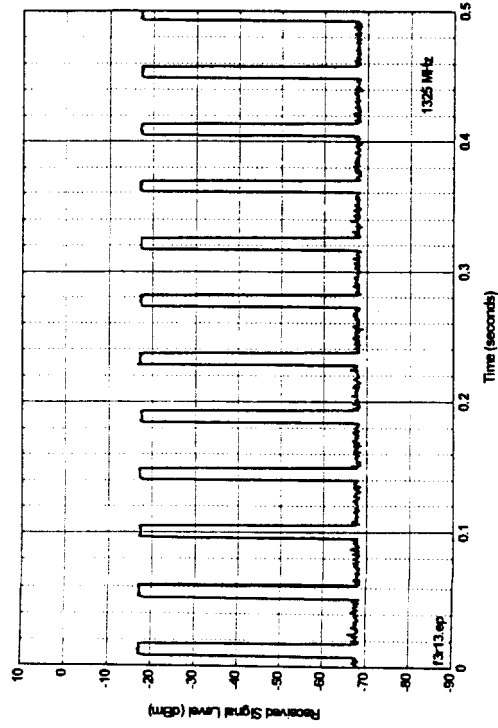


Figure 8.22. Device B, 16-kb/s mode, 3-MHz IF bandwidth, positive peak detector.

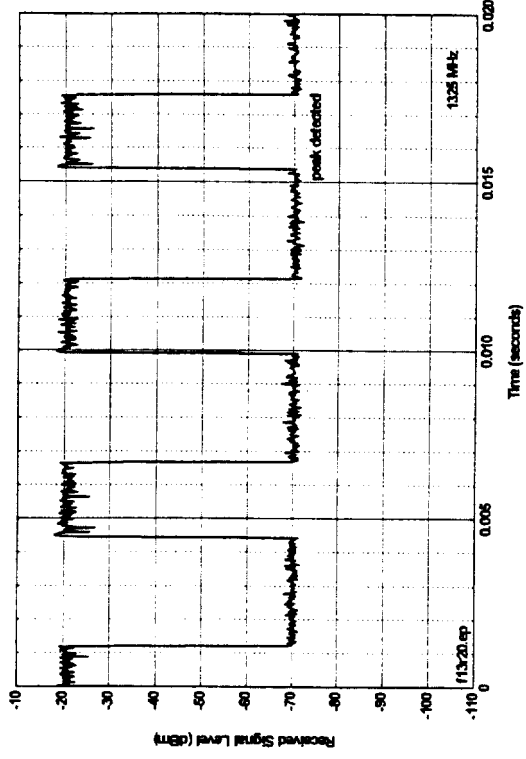


Figure 8.23. Device B, 128-kb/s mode, 3-MHz IF bandwidth.

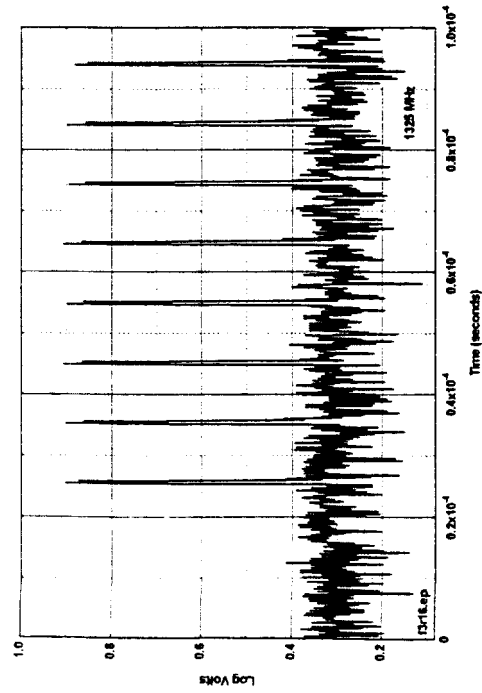


Figure 8.24. Device B PRR waveform, 16-kb/s mode, external detector.

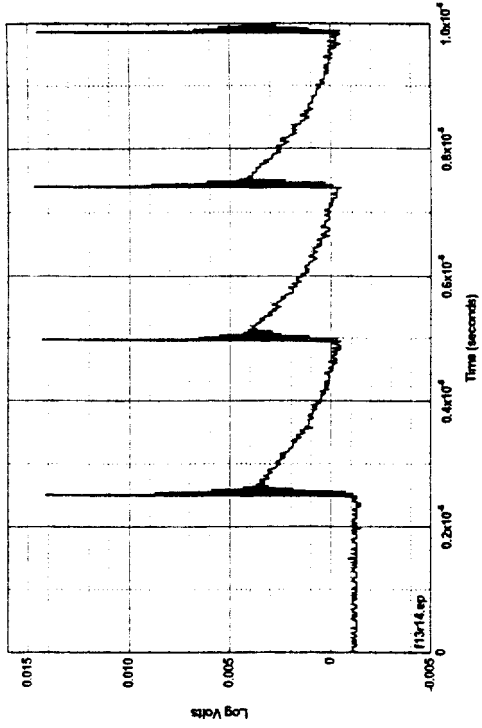


Figure 8.25. Device B PRR waveform, 128-kb/s mode, external detector.

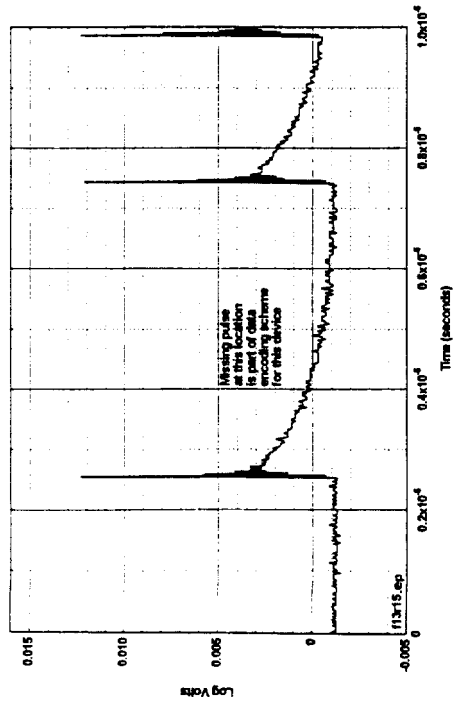


Figure 8.26. Device B, waveform showing on-off modulation, 128-kb/s mode.

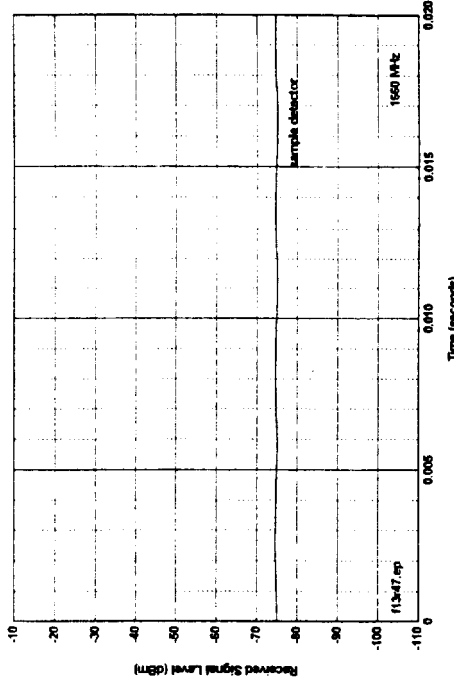


Figure 8.27. Device B, 128-kBit/second mode, 3 MHz BW, 10-Hz video (Part 15-like).

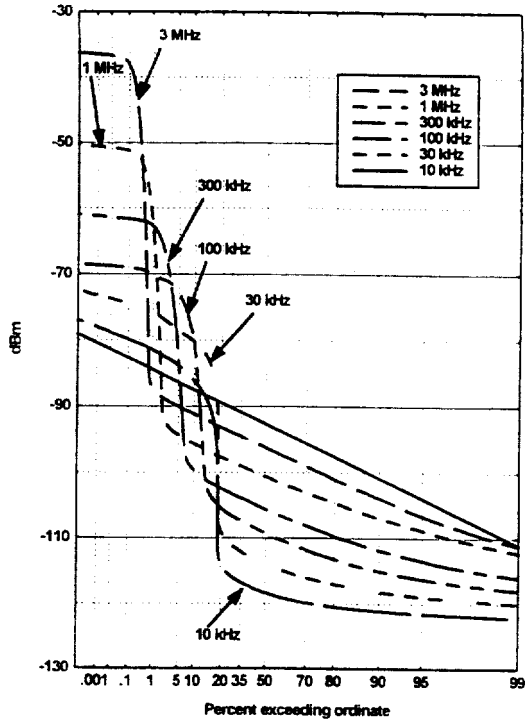


Figure 8.28. Device B APDs, 16 kb/s.

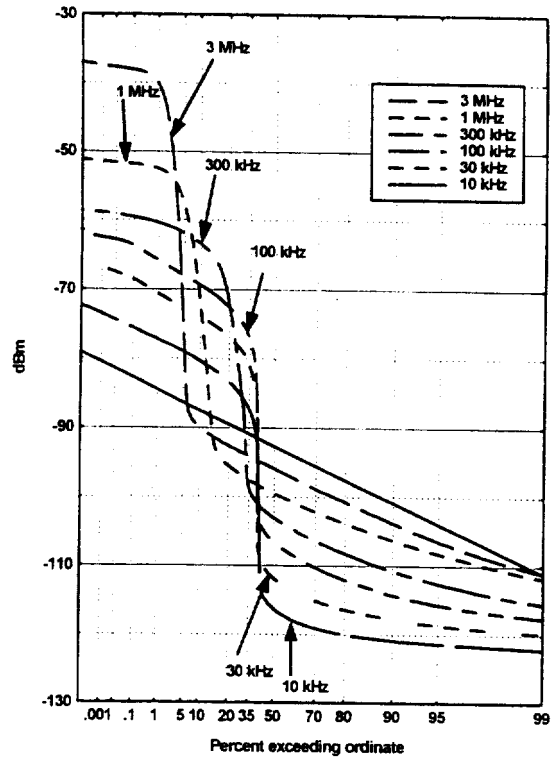


Figure 8.29. Device B APDs, 128 kb/s.

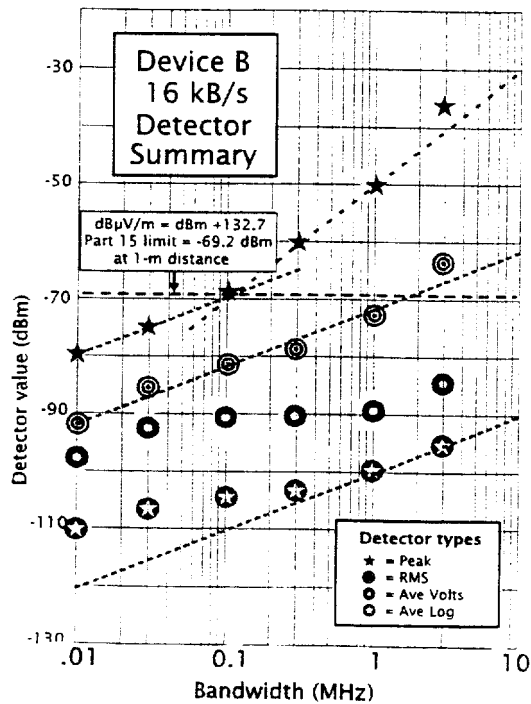


Figure 8.30. Device B detector summary, 16kb/s.

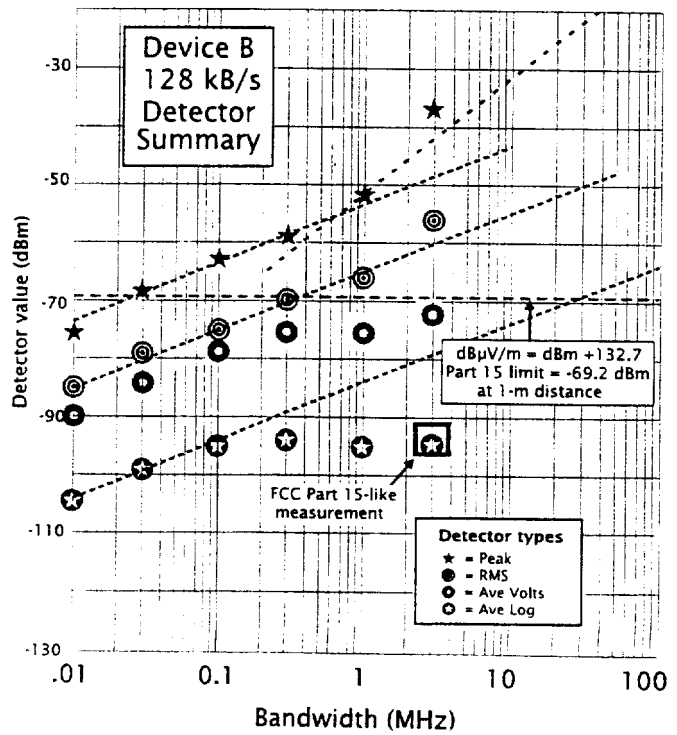


Figure 8.31. Device B detector summary, 128 kb/s.

8.3.3 Summary of Device C Measurements

Device description. Device C transmits an ungated 2-MHz PRR pulse train over the 1-5 GHz range. Device C uses a "relative" dithering technique. This dithering technique uses only a small amount of pulse delay (in this case, 1.25% delay out of 500 ns average pulse spacing), but timing is referred to the preceding pulse instead of being referred to a fixed time base. Figures 8.32 to 8.35 show how a continually larger timing variation builds up over elapsed time, until the 1.25% delay (494-500 ns) for individual pulse-to-pulse spacing covers the entire pulse-to-pulse interval.

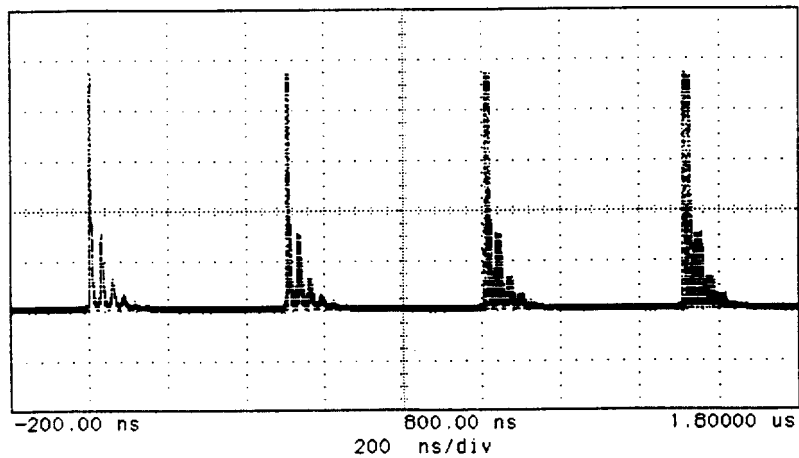


Figure 8.32. Device C dither at starting point.

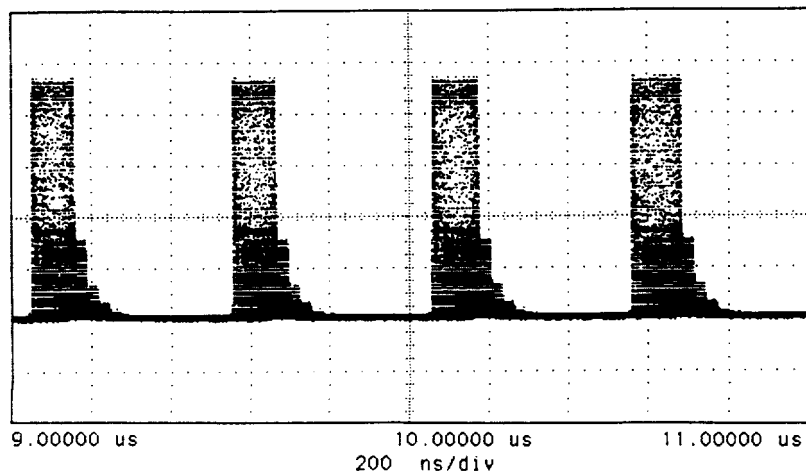


Figure 8.33. Device C dither 20 pulses after zero point.

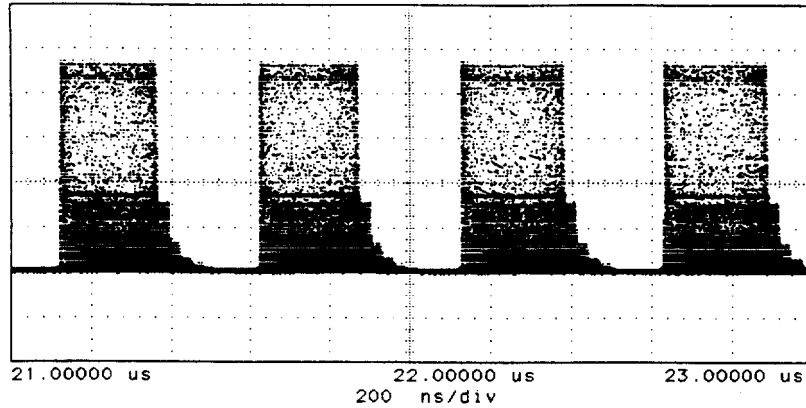


Figure 8.34. Device C dither 44 pulses after zero point

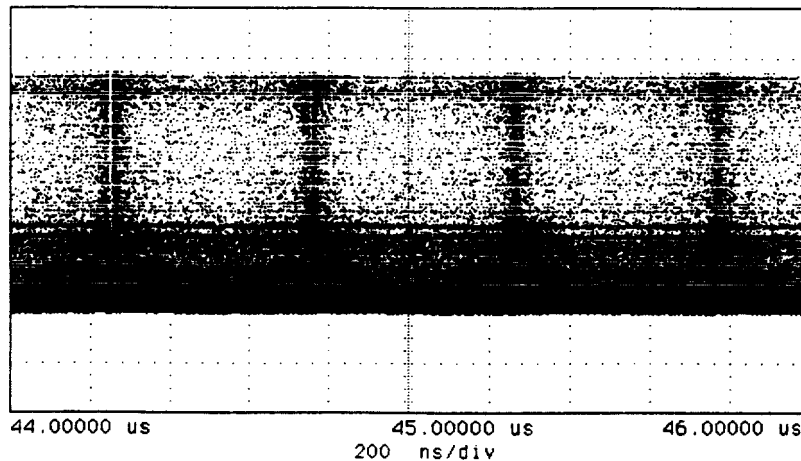


Figure 8.35. Device C dither 90 pulses after zero point

Full-bandwidth pulse shape. Figure 8.36 shows a complex pulse with extended ringing.

FFT emission spectra. Figure 8.37 shows a well-defined emission about 600 MHz wide and centered at about 1800 MHz. The calculated peak radiated field strength is approximately 86 dB μ V/m in a 20-MHz bandwidth..

Narrowband peak emission spectra. Figure 8.38 shows emission spectra with a peak about 700 MHz wide, centered at about 1800 MHz, though the details appear somewhat different from the FFT spectrum. The 20-MHz bandwidth measurements show a measured peak field strength of 87 dB μ V/m, closely matching the FFT spectrum.

Spectrum fine structure. Figure 8.39 shows a subtle set of fine structures related to the 2-MHz average PRR. The relative dithering technique appears to be effective in eliminating 2-MHz discrete spectral lines that extend above the surrounding spectrum. The signals at all frequencies

appear to have about the same maximum power, with a mix of amplitudes that are distributed across a range between the maximum and as much as 30 dB below the maximum. However, there is a pattern of higher-than-average-power frequencies repeated every 2 MHz, where the average signal power is maximized by spending less time at the lower amplitudes. These higher-than-average-power frequencies were designated "on-spectral-lines" frequencies, and intermediate frequencies with less average power were designated "between-spectral-lines" frequencies.

Bandwidth progression stairsteps. Figure 8.40 shows a bandwidth progression measurement made at an "on-spectral-lines" frequency. This measurement shows impulsive behavior at 3-MHz bandwidth, CW-like results for bandwidths between 100 kHz and 1 MHz, and noise-like behavior for narrower bandwidths.

Gating, PRR, and modulation. Figure 8-41 shows a measurement of the Device C pulse train, which exhibits no obvious pulse position modulation. Figures 8-42 and 8-43 show the modulated IF waveforms at 1-MHz and 100-kHz bandwidths. Surprisingly, the 100-kHz waveform contains much more amplitude modulation than the 1-MHz waveform.

APDs. APDs were measured at between-spectral-lines and on-spectral-lines frequencies - Figures 8-44 and 8-45, respectively. Measurements for the between-spectral-lines case were also made using 10-MHz and 20-MHz bandwidths.

Detector summaries. The two APDs and the corresponding detector summaries (Figures 8-46 and 8-47) show some interesting results. The two dashed lines on each detector summary are drawn as best-fit trend lines for the RMS detectors for the on-spectral-lines and between-spectral-lines measurements, showing about 2.5-dB difference between the two cases. The 3-MHz on-spectral-lines RMS value drops to the between-spectral-lines trend line, showing that the effect of the relatively narrow bandwidth concentration of on-spectral-lines energy disappears when the measurement bandwidth is widened beyond the 2-MHz fine structure.

The between-spectral-lines detector summary shows a large divergence between different detector values at 100-kHz bandwidth, including a 15-dB difference between average logarithm and RMS and a 27-dB difference between average logarithm and peak. The minimum difference between detector values occurs at 1-MHz bandwidth, where there is only a 6-dB difference between average logarithm and peak values. These results are particularly interesting (and somewhat counterintuitive) because they illustrate a UWB modulation technique that produces impulse-like results (i.e., wide divergence between detector values) at lower bandwidths and CW-like results at higher bandwidths. The proposed FCC Part 15 limits, however, assume that a UWB signal will appear more CW-like at lower bandwidths (average limit specified in 1-MHz bandwidth), and more impulsive at higher bandwidths (peak limit specified in $B = 50$ MHz).

FCC Part 15 measurements. Part 15 measurements were made at the "on-line" frequency using a 300-Hz video filter, which produced a signal with about 0.5 dB peak-to-peak ripple and a peak amplitude of -74 dBm. This compares with a computed average logarithm of -74.2 dBm.

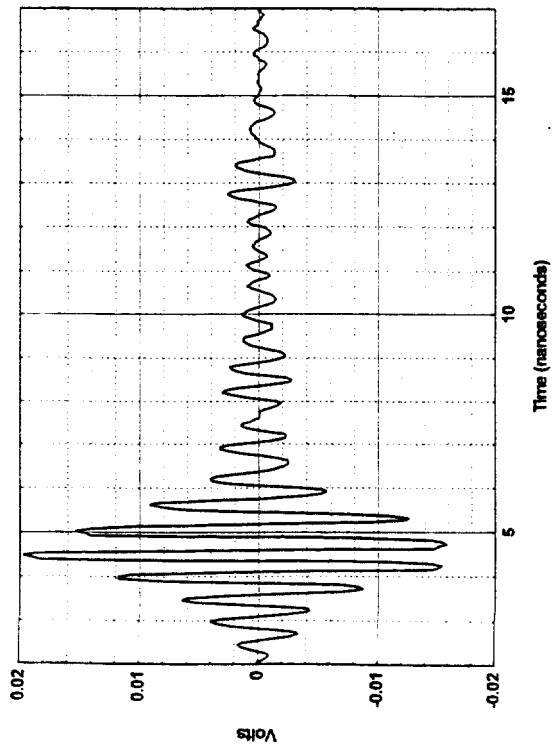


Figure 8.36. Device C full bandwidth pulse shape.

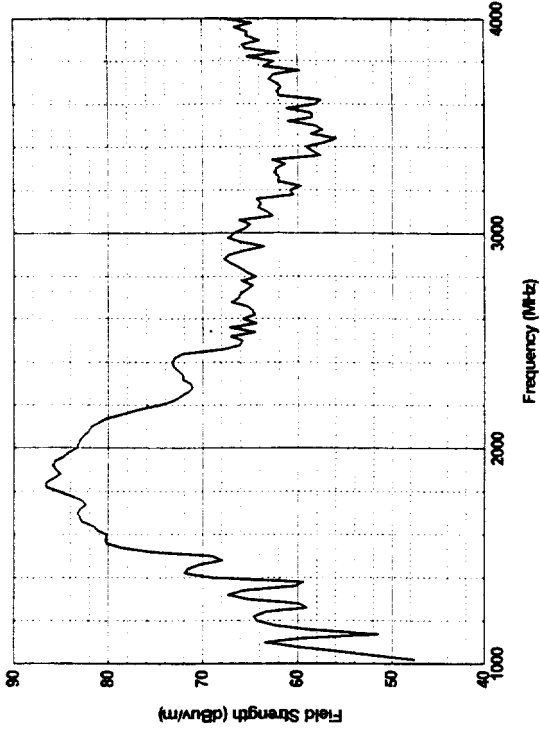


Figure 8.37. Device C, radiated peak field strength at 1 m, $\Delta f = 20$ MHz.

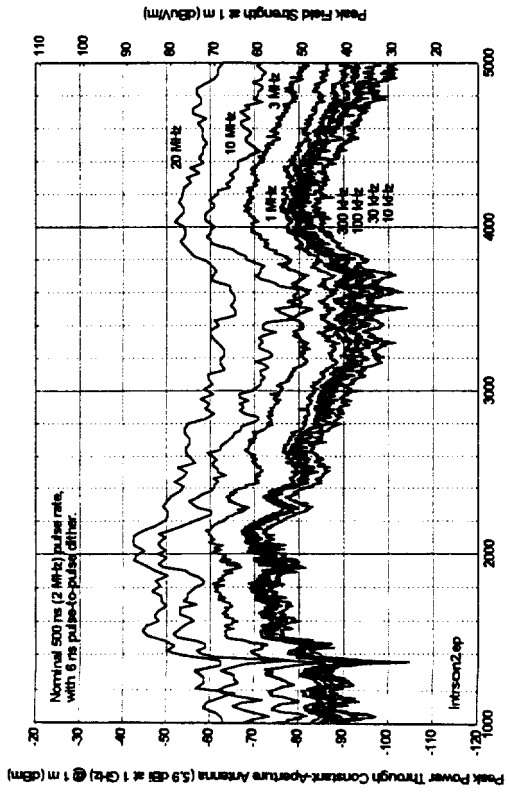


Figure 8.38. Device C spectra in multiple bandwidths.

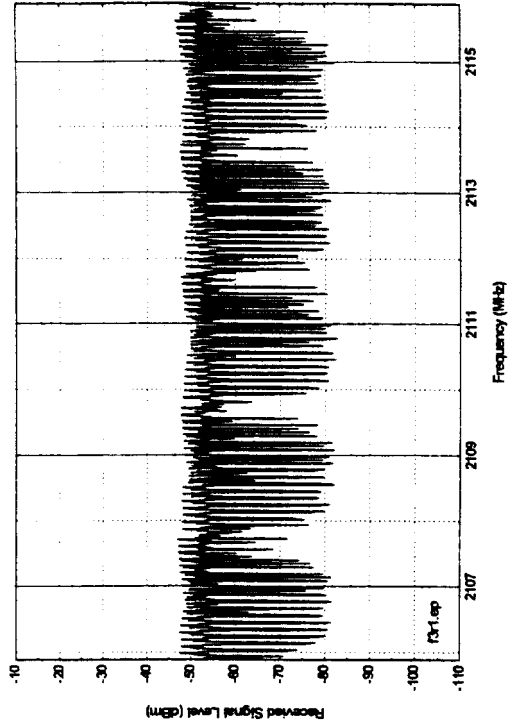


Figure 8.39. Device C, peak-detected to show spectral line patterns in noise.

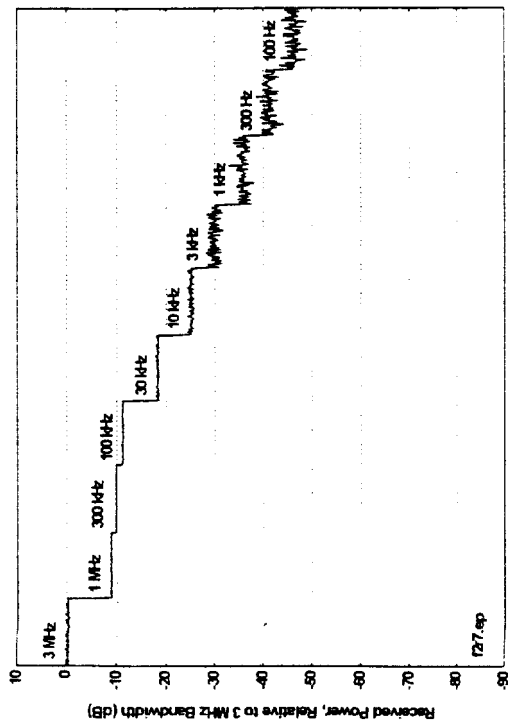


Figure 8.40. Device C, peak bandwidth progression staircase.

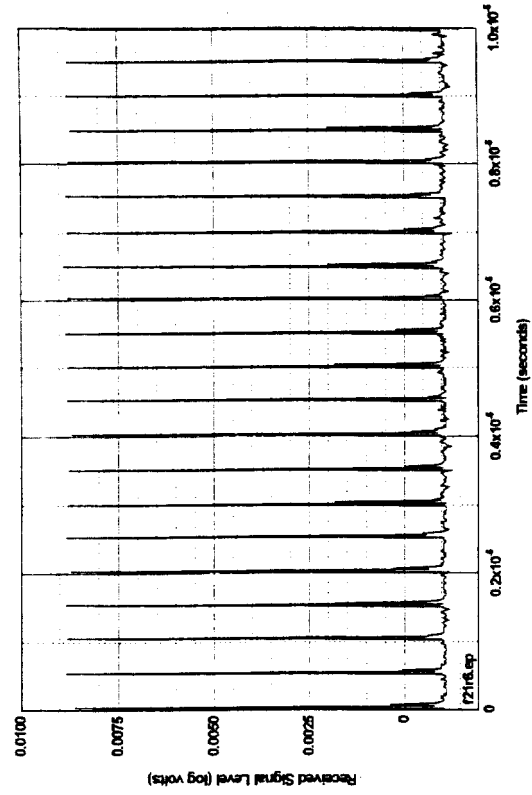


Figure 8.41. Device C, pulse train waveform for 10 microseconds, external detector.

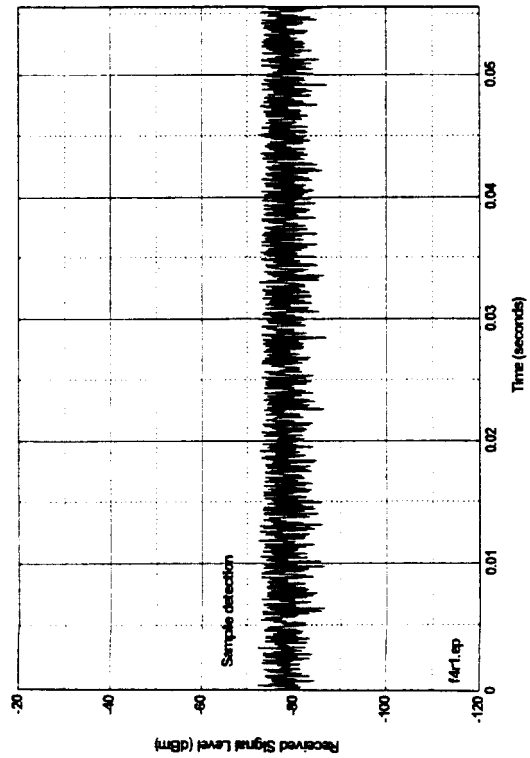


Figure 8.42. Device C, time waveform in 55 ms, 3-MHz IF bandwidth.

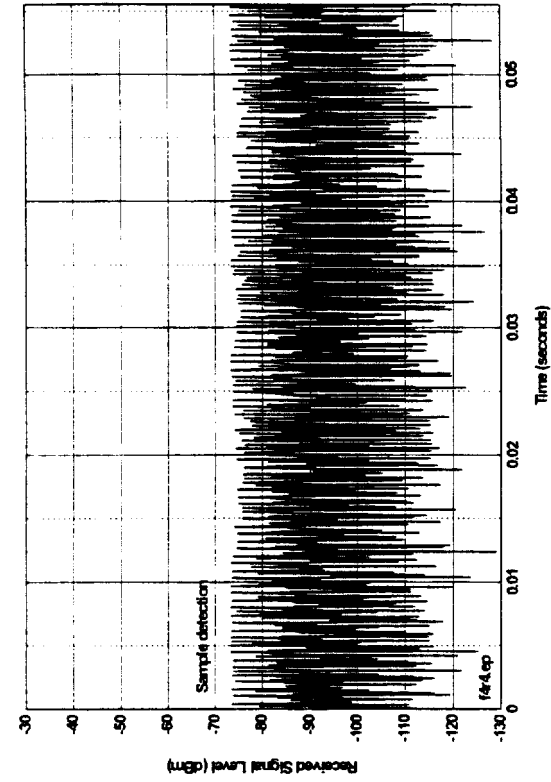


Figure 8.43. Device C, time waveform in 55 ms, 100-kHz IF bandwidth.

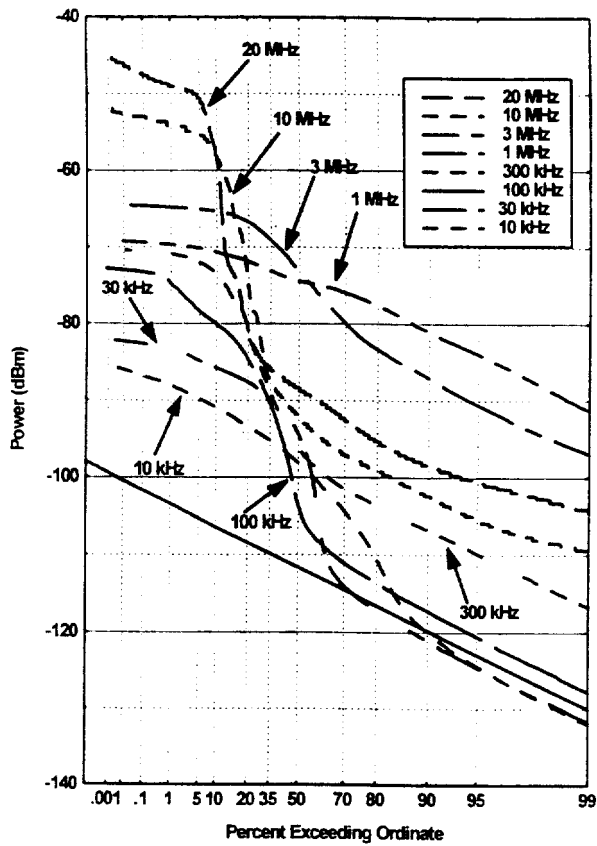


Figure 8.44. Device C APDs, between spectral lines.

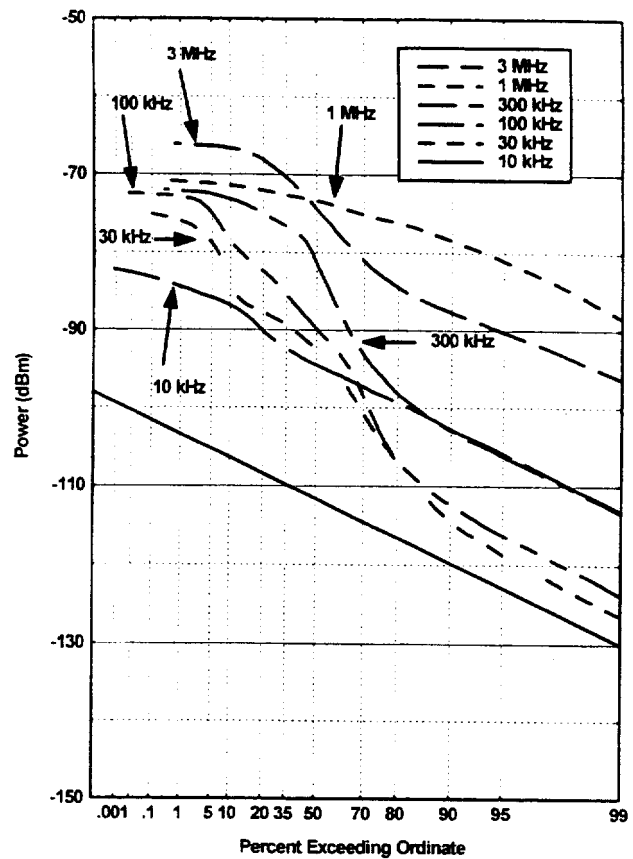


Figure 8.45. Device C APDs, on spectral lines.

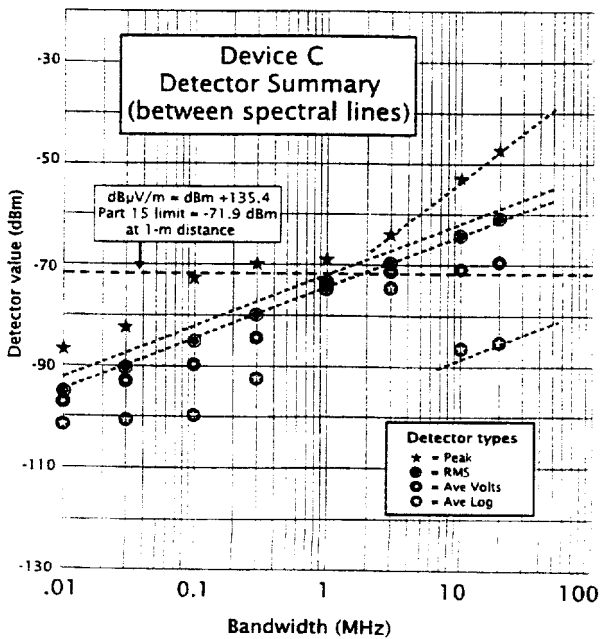


Figure 8.46. Device C, detector summary (between spectral lines).

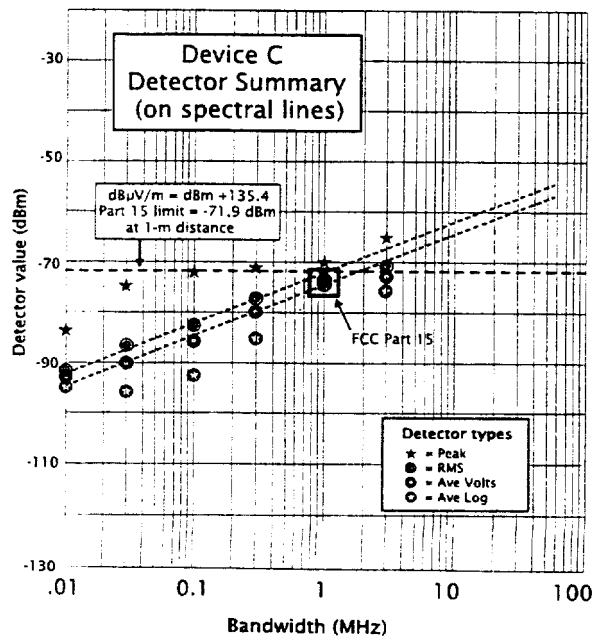


Figure 8.47. Device C, detector summary (on spectral lines)

8.3.4 Summary of Device D Measurements

Device Description: Device D operates with basic PRRs of 1 MHz, 5 MHz, and 10 MHz, with gating duty cycles available between 25% and 100% (continuously on). A fixed 25% dither is applied, using an absolute time base in all modes. The device was measured in four modes: 1-MHz PRR, 25% gated duty cycle; 1-MHz PRR, 100% gated duty cycle; 10-MHz PRR, 25% gated duty cycle; and 10-MHz PRR, 100% gated duty cycle. The gating cycle for both PRRs utilized a 2-ms "on" period and a 6-ms "off" period. This data transmission device was measured without transmitting any actual data.

Full-bandwidth pulse shape and FFT spectrum. The Device D radiated full-bandwidth pulse shape (Figure 8.48) was used to compute an FFT peak spectrum over the 1-4 GHz range (Figure 8.49).

Narrowband peak emission spectra. Figures 8.50-8.53 contain spectrum measured for each of four Device D operating modes. These spectra compared closely in shape and amplitude with the FFT spectrum. Figure 8.53 included measurements made in a 20-MHz bandwidth, which show close agreement (within 1-2 dB) with the FFT values computed in a 20-MHz bandwidth.

Bandwidth progression staircase. The stair-step bandwidth progression graphs (Figures 8.54-8.57) were measured at a frequency near 1560 MHz and show substantial differences between the 1-MHz PRR and the 10-MHz PRR modes. These differences are likely caused by the higher power and greater frequency separation of the discrete spectral lines in the 10-MHz PRR modes.

Spectrum fine structure. Details of the spectrum fine structure showed strong lines with 1-kHz spacing in the 1-MHz PRR mode (Figure 8.58) and 10-kHz spacing in the 10-MHz PRR mode (Figure 8.59). It is not known whether these lines would be present with transmission of actual data. Figure 8-60 shows pulse-position modulation, measured in a 10-MHz bandwidth.

APDs. The APDs are shown in Figures 8.62 to 8.65. The non-gated modes (100% gating) appear like Gaussian noise for bandwidths less than the PRR and appear impulse-like for bandwidths larger than the PRR. The gated modes show clear break-points at the 25% point, with measurement system noise present for the remaining 75% of the duration.

Detector summary. The detector summaries (Figures 8.66 to 8.69) show that the ungated modes appeared similar to Gaussian noise for bandwidths less than the PRR. For all narrower bandwidths, peak values were about 10-dB greater than the RMS, and the average voltage and average logarithm were tightly clustered within a few dB less than the RMS. All of the detector functions followed a $10 \log_{10} B$ trend line. The corresponding trend lines were 8-10 dB higher for the 10-MHz PRR than for the 1-MHz PRR mode. Only when the bandwidth was greater than the PRR, did the detector values at a bandwidth begin to diverge. The peak values then followed a $20 \log_{10} B$ trend. The average logarithm and average voltage decreased substantially at larger bandwidths, when pulses did not overlap and system noise was momentarily the only signal.

The gated modes provided peak values identical to the corresponding ungated (i.e., 100%) modes. The gated RMS values were approximately 6 dB lower than those of the corresponding ungated modes, as expected when the total number of impulses was decreased by 75%. The gated mode average logarithm dropped to within a few dB of system noise (present 75% of the time), with the 10-MHz PRR average logarithm being 1-2 dB higher than the 1-MHz logarithm.

FCC Part 15 Measurements. Part 15 measurements for the ungated 1-MHz PRR and 10-MHz PRR modes matched the average logarithms at -84 dBm and -74 dBm, respectively. Part 15 measurements for the gated modes were -100 dBm and -97 dBm for the 1-MHz PRR mode and 10-MHz PRR mode (Figure 8.61), respectively. The 1-2 dB discrepancy between Part 15 and average logarithm for gated modes was caused by insufficient video filtering of the 8 ms gating cycle, which allowed 2-3 dB of ripple on the video filter output.

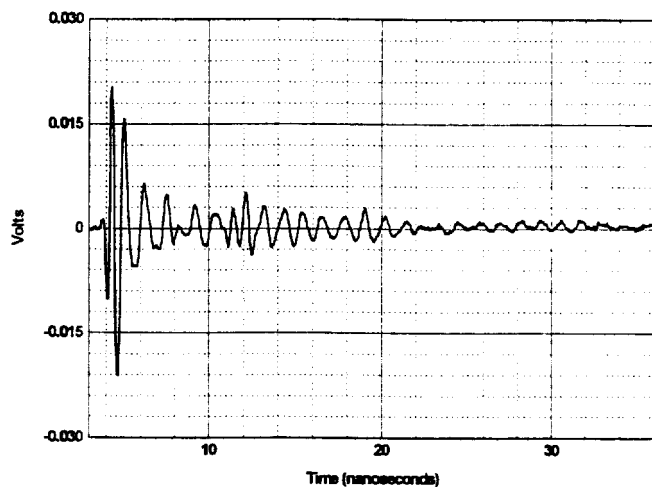


Figure 8.48. Device D radiated full-bandwidth pulse shape

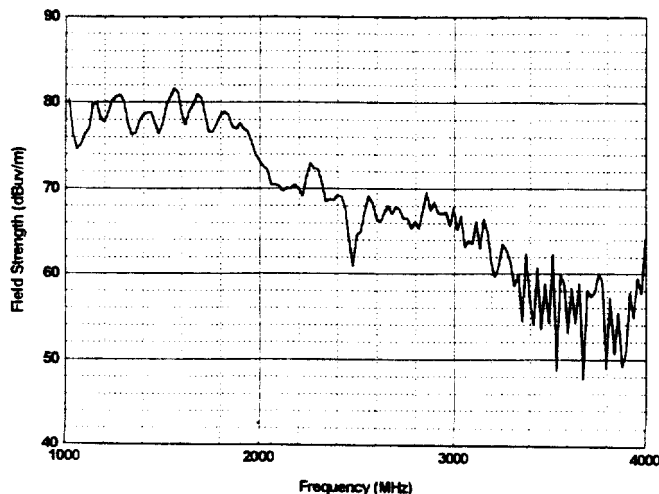


Figure 8.49. Device D, radiated peak field strength at 1 m, $\Delta f = 20$ MHz.

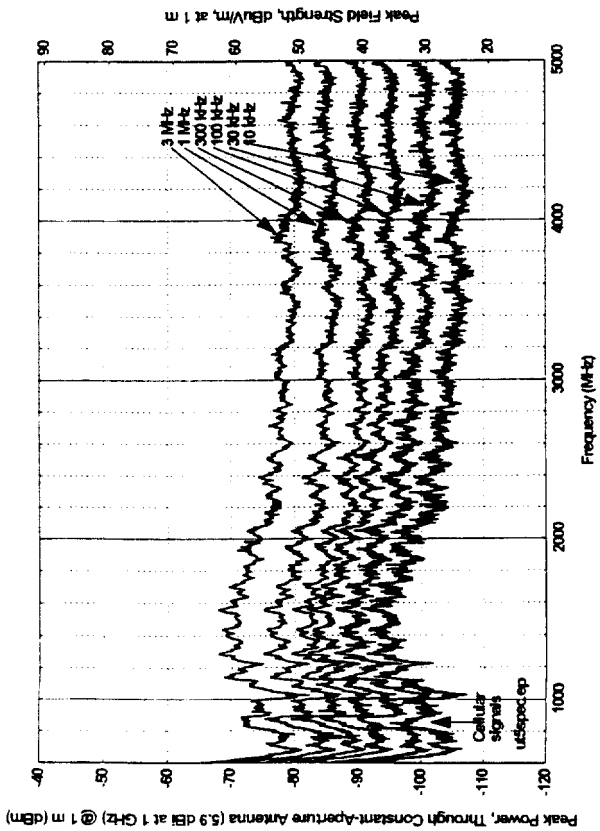


Figure 8.50. Device D spectra, 1-MHz PRR, 25% gating.

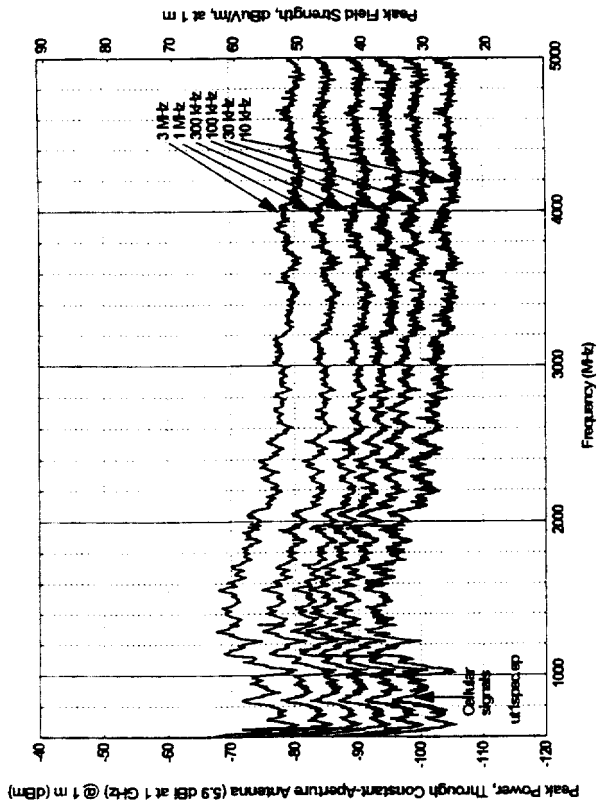


Figure 8.51. Device D spectra, 1-MHz PRR, 100% gating.

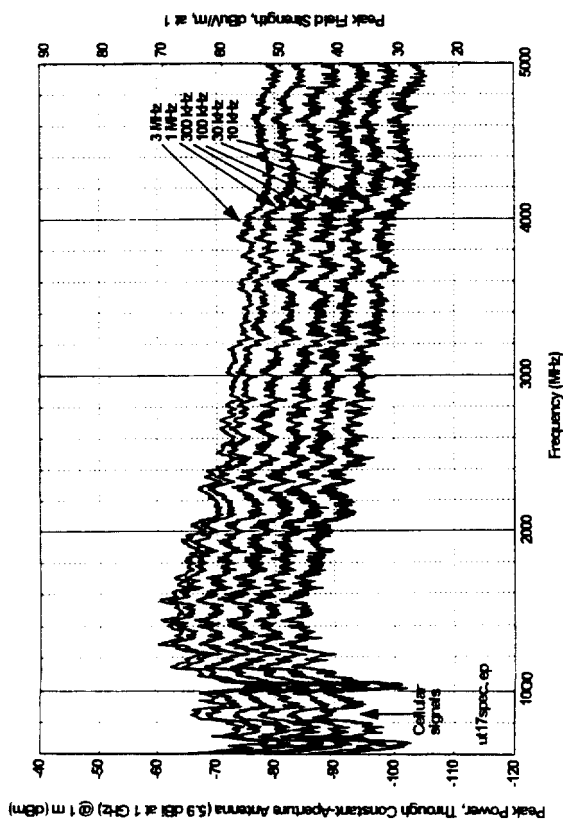


Figure 8.52. Device D spectra, 10-MHz PRR, 25% gating.

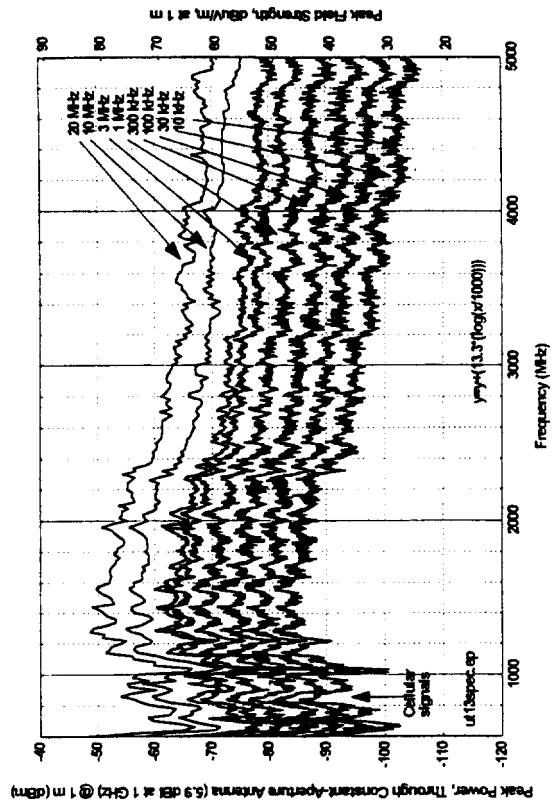


Figure 8.53. Device D spectra, 10-MHz PRR, 100% gating.

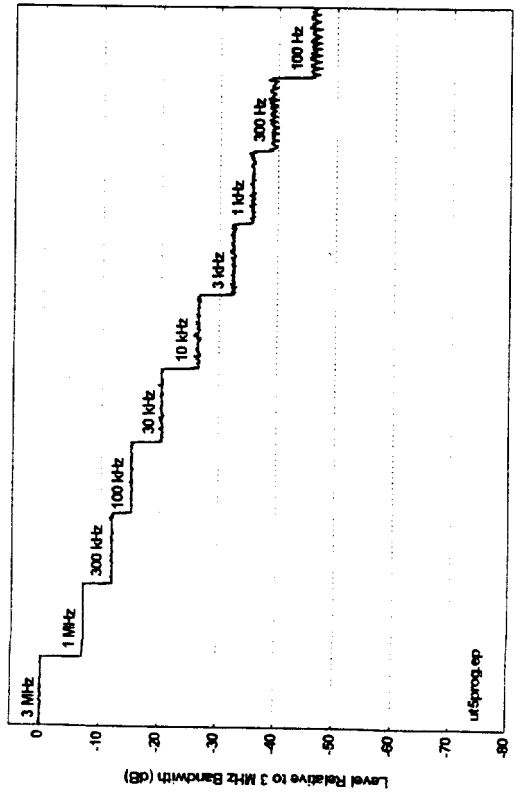


Figure 8.54. Device D bandwidth progression staircase,
1-MHz PRR, 25% gating.

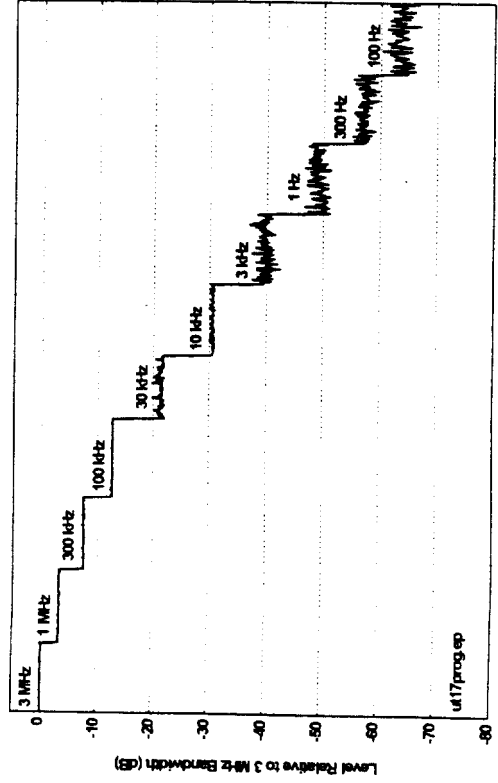


Figure 8.56. Device D bandwidth progression staircase,
10-MHz PRR, 25% gating.

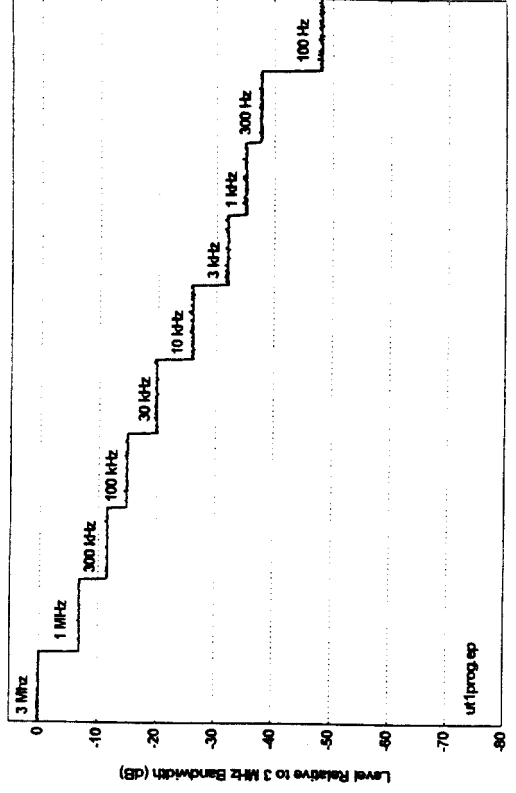


Figure 8.55. Device D bandwidth progression staircase,
1-MHz PRR, 100% gating.

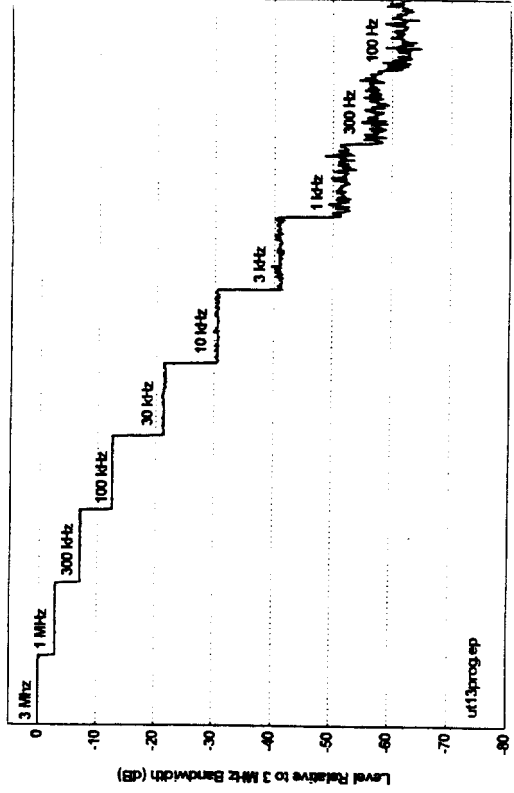


Figure 8.57. Device D bandwidth progression staircase,
10-MHz PRR, 100% gating.

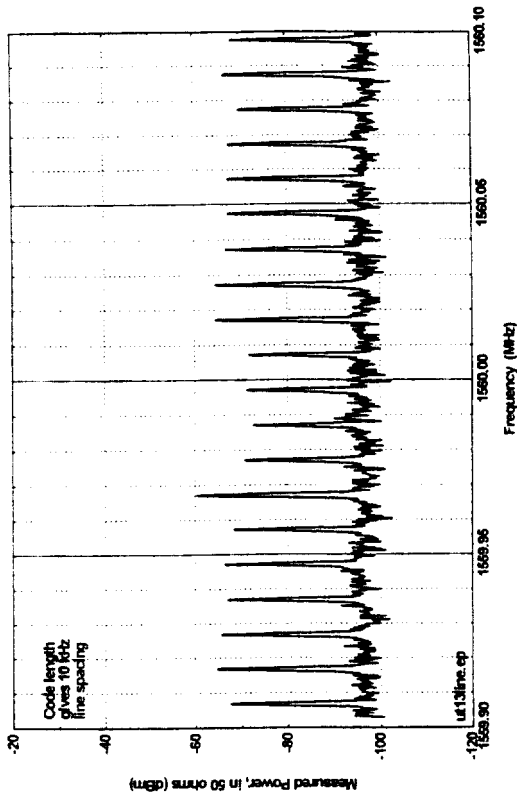


Figure 8.59. Device D 10-kHz emission lines, 10-MHz PRR, 100% gating.

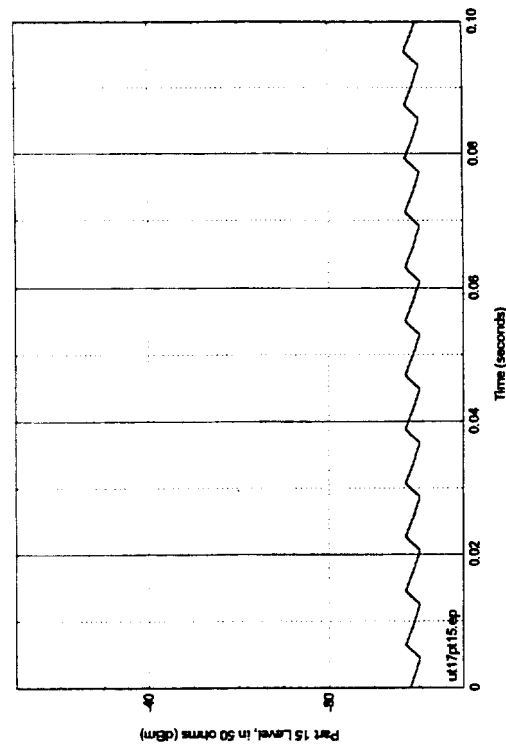


Figure 8.61. Device D, 10-MHz PRR, 25% gating, Part 15 measurement showing ripple in 10-Hz video BW.

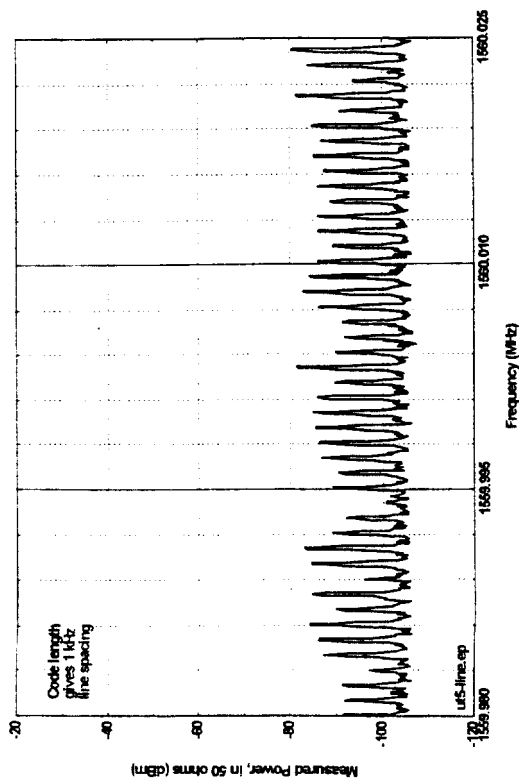


Figure 8.58. Device D 1-kHz emission lines, 1-MHz PRR, 25% gating.

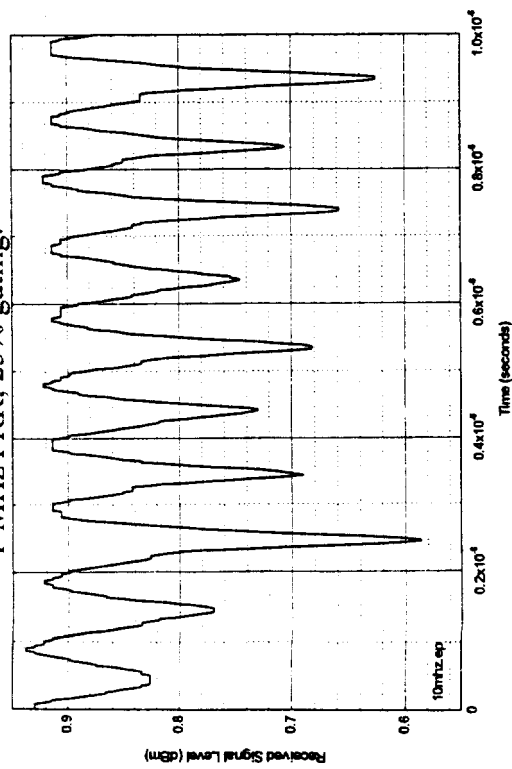


Figure 8.60. Device D waveforms, 10-MHz IF, 10-MHz PRR, 100% gating, 25% dither, showing pulse position modulation.

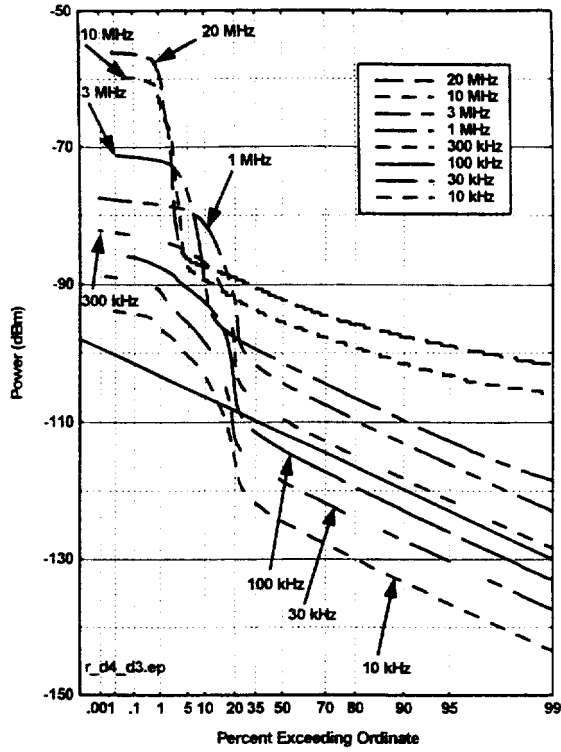


Figure 8-62. Device D APDs,
1-MHz PRR, 25% gating.

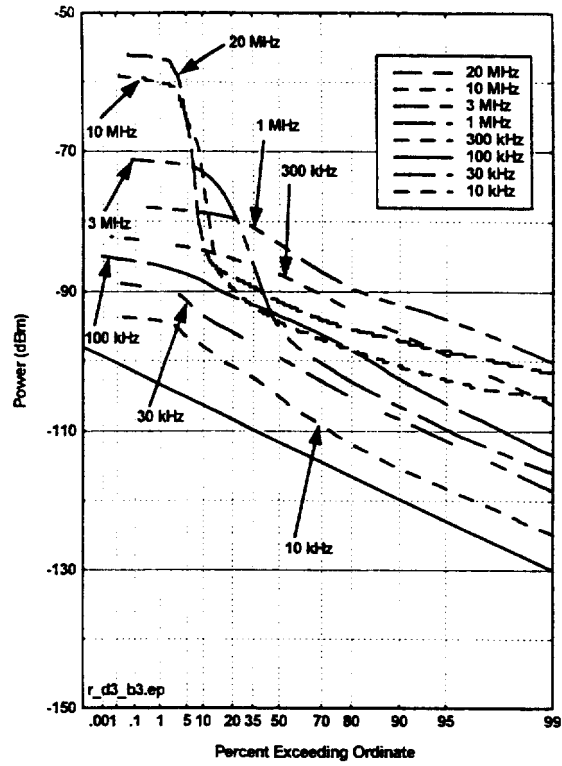


Figure 8.63. Device D APDs,
1-MHz PRR, 100% gating.

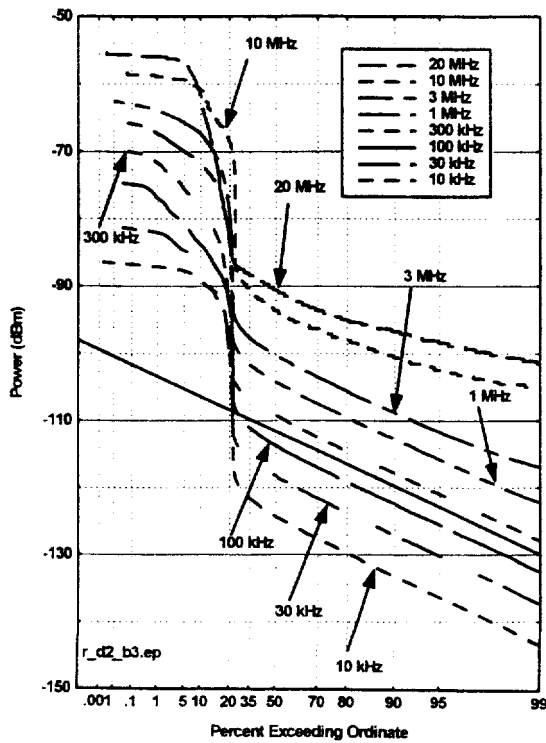


Figure 8.64. Device D APDs,
10-MHz PRR, 25% gating.

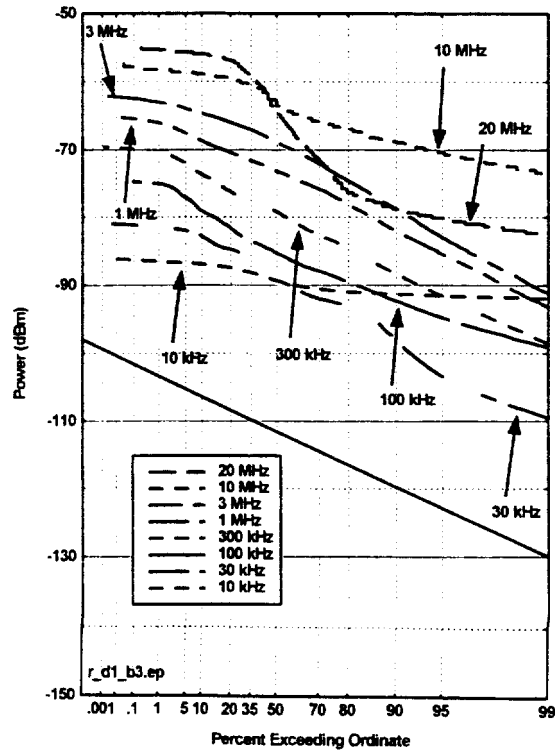


Figure 8.65. Device D APDs,
10-MHz PRR, 100% gating.

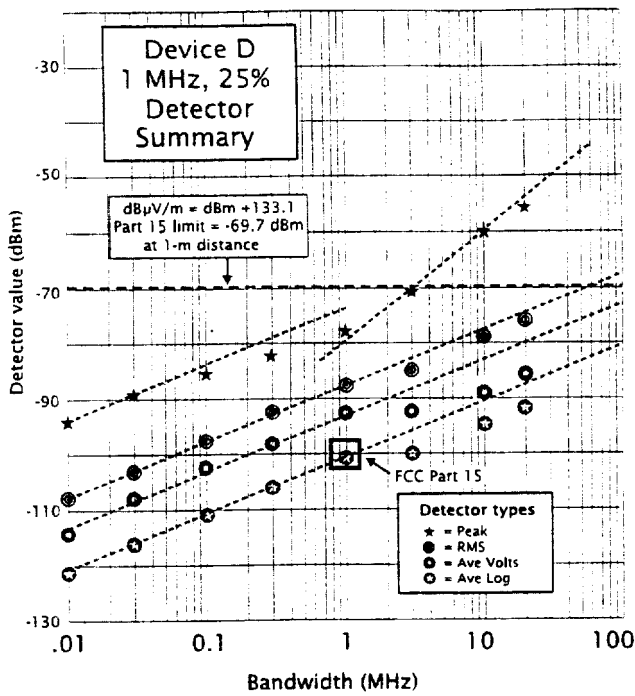


Figure 8.66. Device D detector summary, 1-MHz PRR, 25% gating.

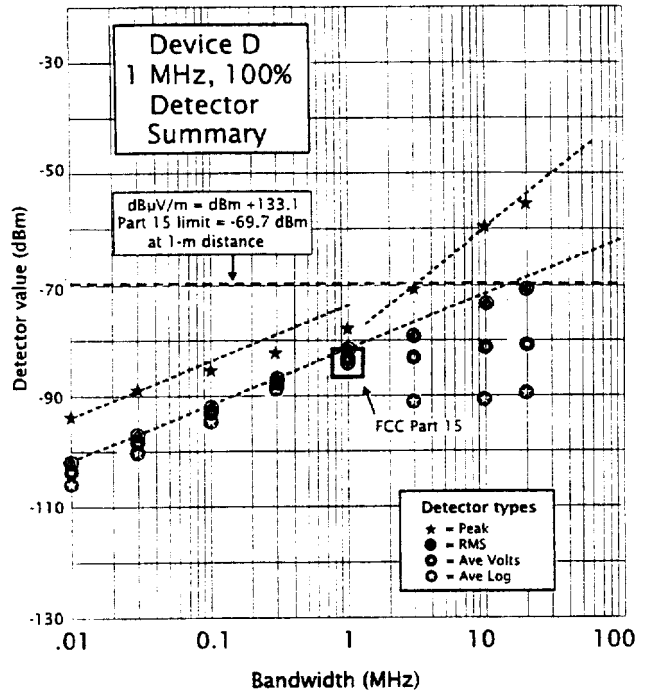


Figure 8.67. Device D detector summary, 1-MHz PRR, 100% gating.

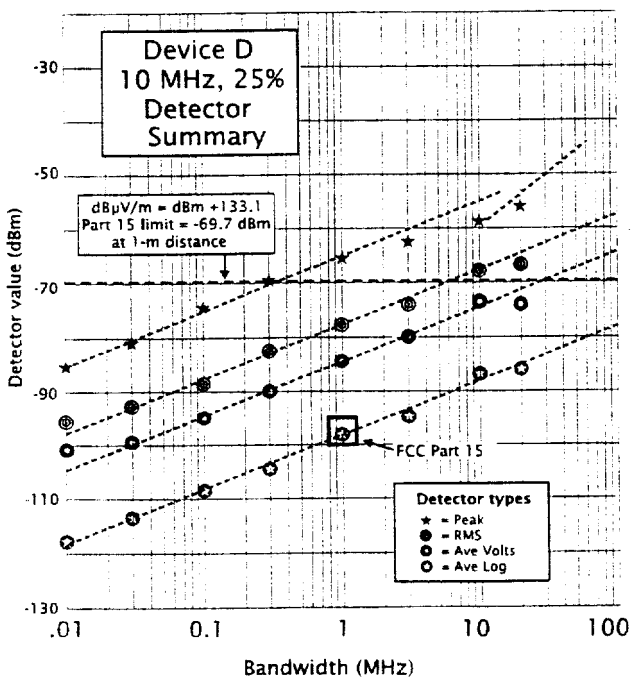


Figure 8.68. Device D detector summary, 10-MHz PRR, 25% gating.

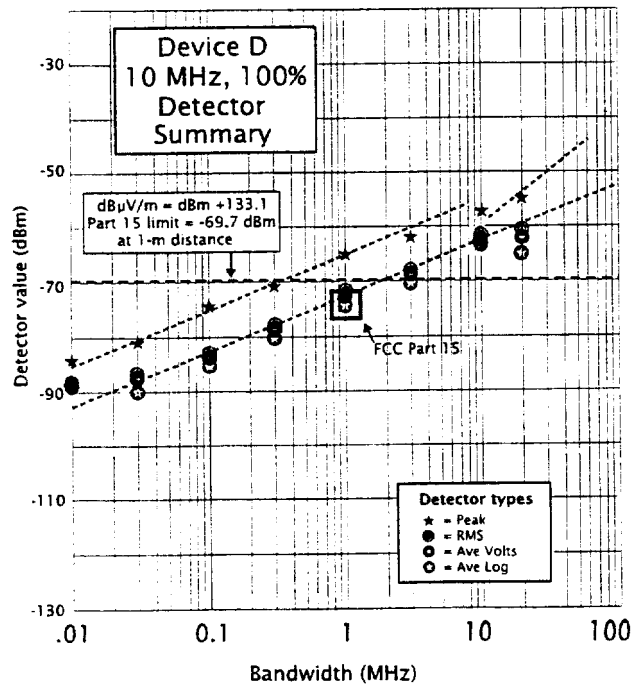


Figure 8.69. Device D detector summary, 10-MHz PRR, 100% gating.

8.3.5 Summary of Device E Measurements

Device description: Device E is designed to radiate mainly towards the ground. Interchangeable RF heads permitted operation at nominal frequencies of 300 MHz, 900 MHz, and 1500 MHz. Device E is capable of operating with multiple PRRs.

Full-bandwidth pulse shapes. Full-bandwidth pulse shape measurements were made with all three RF heads (Figures 8.69, 8.71, and 8.73), with the Device E antennas aimed directly at the measurement antenna 1 m away. These pulse shapes are very simple, with no additional lobes or extended ringing.

FFT emission spectra. FFT spectra were computed from each of the measured pulse shapes (Figures 8.70, 8.72, and 8.74, respectively).

Narrowband peak emission spectra. Spectrum analyzer measurements were made only with the 1500-MHz head, with Device E resting on a concrete floor, aiming downwards, with the measurement antenna 1 meter away from the edge of Device E and slightly above the floor. The spectrum analyzer measurements signal amplitudes cannot be compared with the FFT spectra because of different measurement conditions.

Bandwidth progression staircase. Figure 8.76 shows the Device E emission spectrum, using the 1500-MHz RF head.

Gating, PRR, and modulation. The mode that was measured included a PRR near 85 kHz and a gating duty cycle of approximately 25 ms on, 6 ms off (Figures 8-78 and 8-79). A distinguishing feature of the Device E spectrum analyzer measurements was relatively low received power, which prevented Part 15 measurements from being made, and which also made it difficult to see some details of the modulation.

APDs. Figure 8.80 show APD measurements for the Device E 1500-MHz RF head.

Detector summary. Figure 8.81 shows a detector summary for Device E. Detector values for bandwidths less than 1 MHz seem to be mostly measurement system noise.

FCC Part 15 measurements. The signal from Device E was apparently below measurement system noise and Part 15 measurements could not be performed.

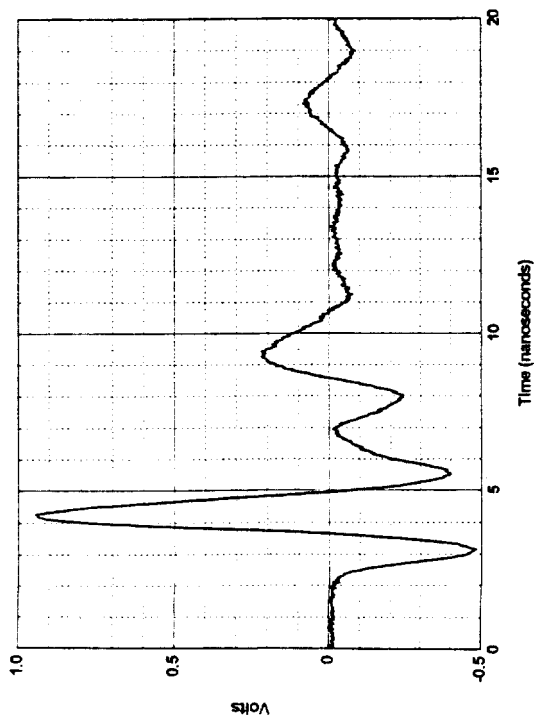


Figure 8.70. Device E full bandwidth pulse shape, 300-MHz RF head, main beam.

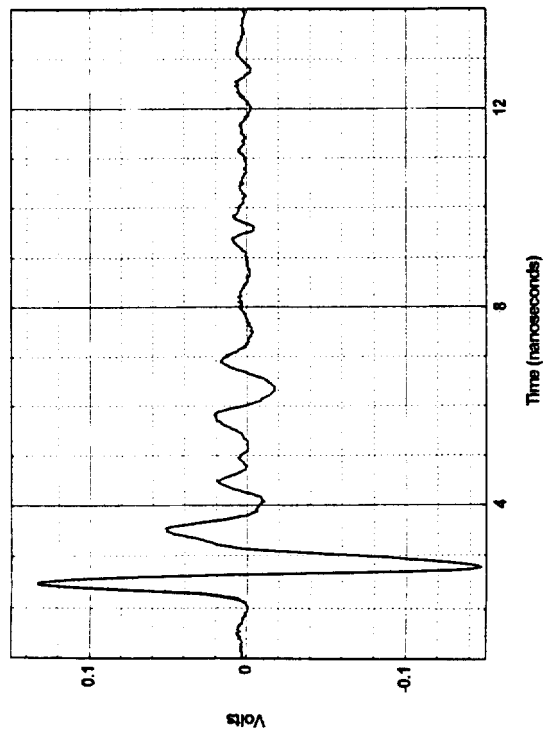


Figure 8.72. Device E full bandwidth pulse shape, 900-MHz RF head, main beam.

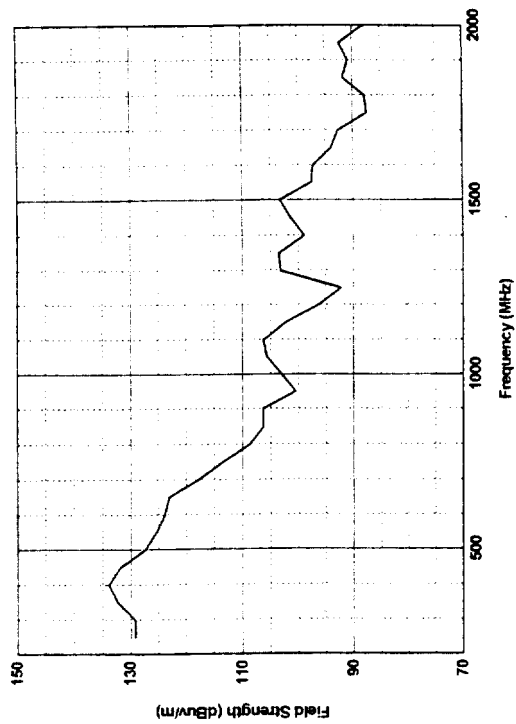


Figure 8.71. Device E, (300-MHz head), peak field strength at 1 m, main beam, $\Delta f = 50$ MHz.

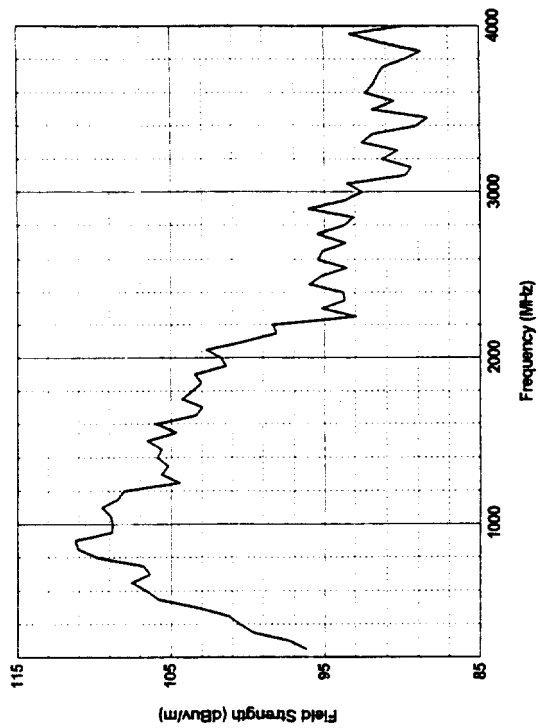


Figure 8.73. Device E (900-MHz head) peak field strength at 1 m, main beam, $\Delta f = 50$ MHz.

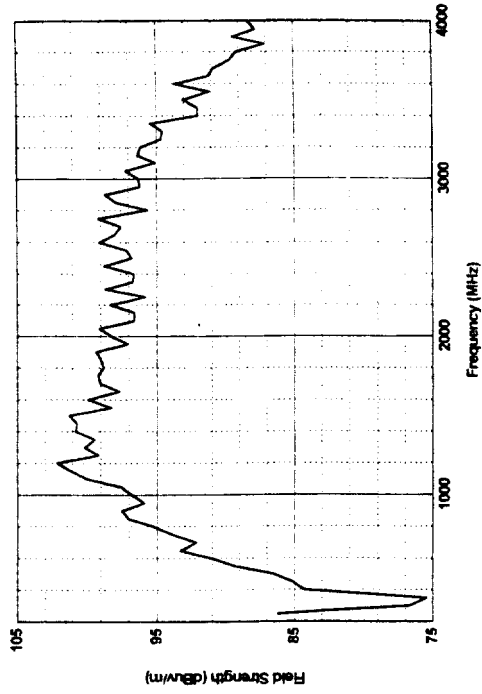


Figure 8.75. Device E (1500-MHz head) peak field strength at 1 m, main beam, $\Delta f = 50$ MHz.

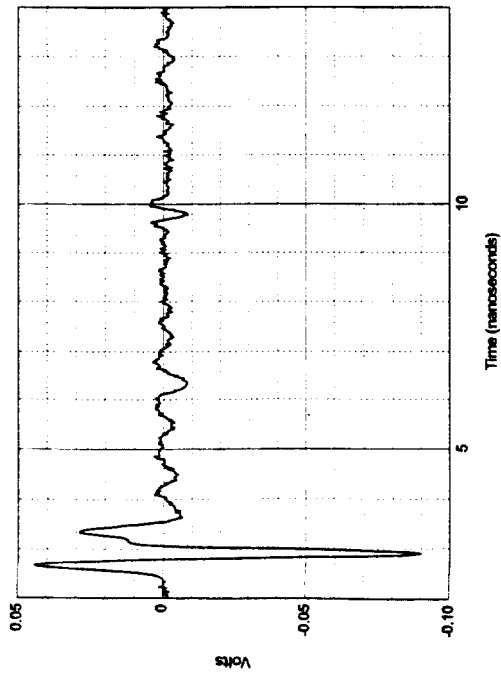


Figure 8.74. Device E full bandwidth pulse shape, 1500-MHz RF head, main beam.

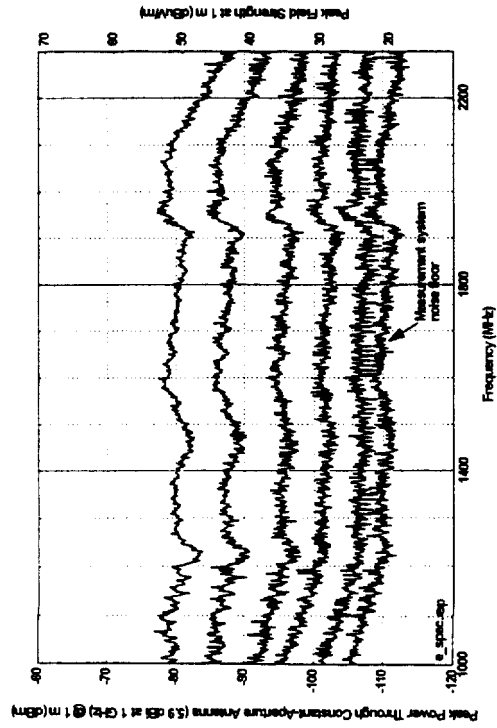


Figure 8.76. Device E 1500-MHz RF head, spectra as a function of measurement bandwidth.

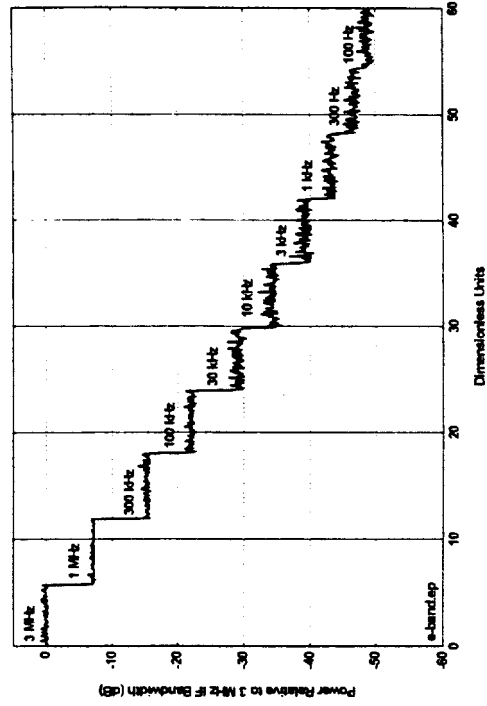


Figure 8.77. Device E 1500-MHz RF head, peak bandwidth progression staircase.

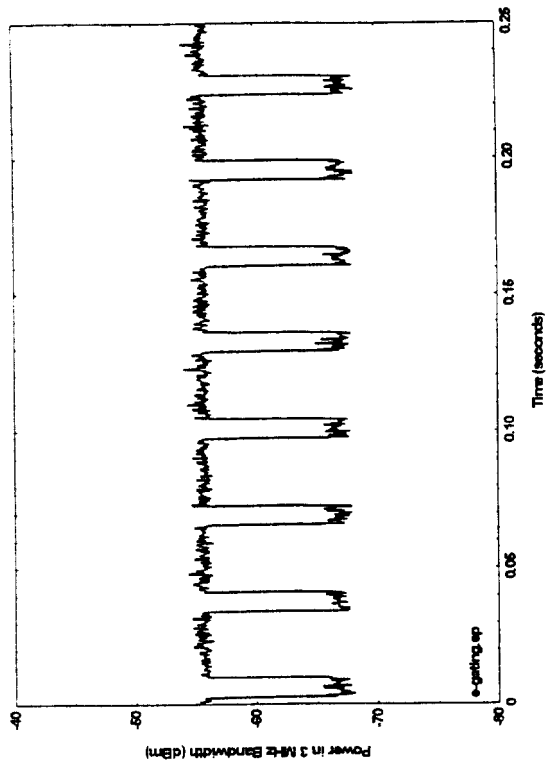


Figure 8.78. Device E pulse train.

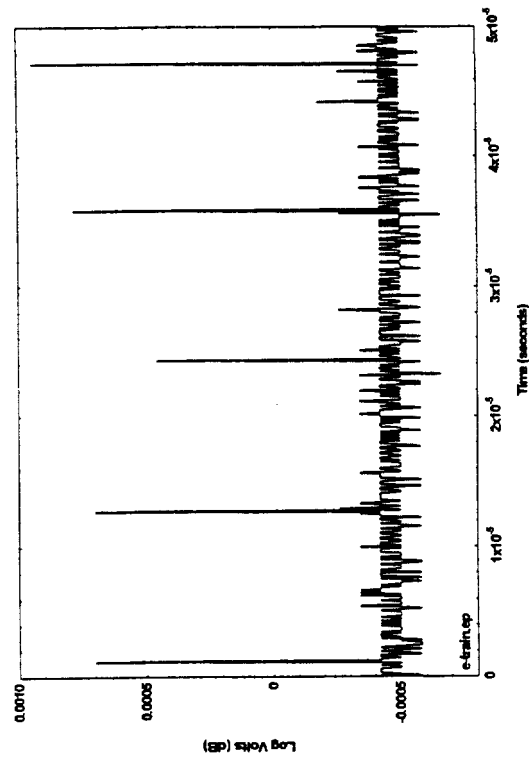


Figure 8.79. Device E gating waveform.

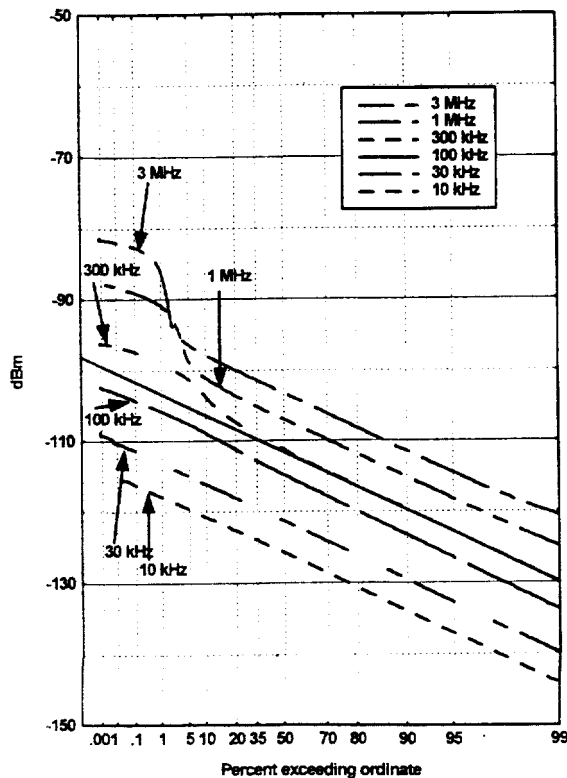


Figure 8.80. Device E APDs.

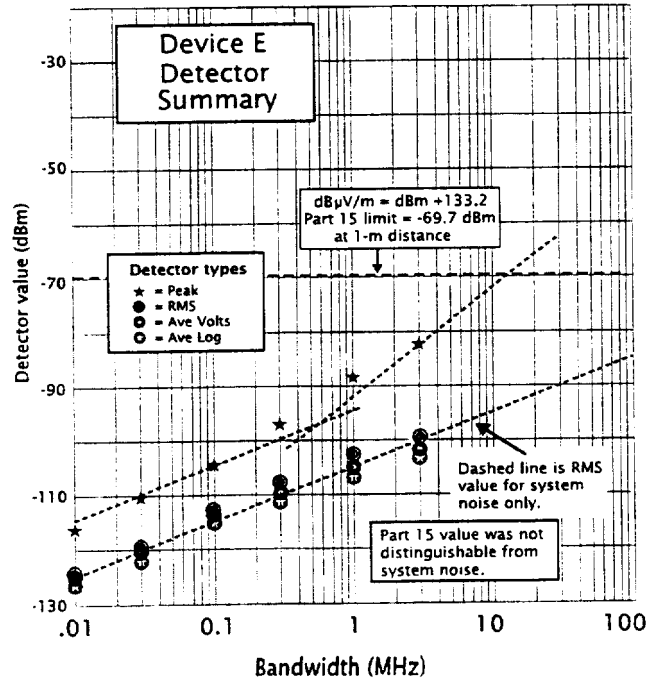


Figure 8.81. Device E, detector summary.

8.3.6 Summary of Electric Drill Measurements

An electric drill is included in the category of Part 15 Incidental Radiators, since it radiates radio frequency energy, although its function does not require the generation of radio frequency signals. The electric drill controls included only an on/off switch (i.e., no electronic speed control), and it was measured without any mechanical loading on the drill shaft.

Full-bandwidth pulse shapes. The random nature of the timing and amplitude of the electrical impulses from the drill made it impossible to use a sampling oscilloscope to measure the emitted impulses. Therefore, no full-bandwidth pulse shape measurements were made, and no FFT spectrum could be derived from the pulse.

Narrowband peak emission spectra. The energy radiated from the electric drill was measured by the spectrum analyzer over the 0.6-5.0 GHz range (Figure 8.82), including a noticeable "bulge" in the 3.1-4.2 GHz range. The highest frequency of measurable signal is not known. The apparent change of amplitudes measured with various bandwidths using the peak detector seems to be about 42 dB for a 2.5-decade change in bandwidth, i.e., a $17 \log_{10} B$ trend line.

Gating, PRR, and modulation. Figure 8.83 shows the gradually building and declining burst of noise that occurs about every 17 ms and is related to the 60 Hz power line frequency.

APDs. Each drill APD in Figure 8.84 appears to be divided into impulsive and noise-like parts, with the noise-like portion determined by measurement system noise and following a $10 \log_{10} B$ rule. The impulsive portion, unlike typical UWB devices, assumes a steep, straight-line slope without any hint of a plateau. The 1-MHz and 3-MHz APDs seem to develop an even steeper slope at the low-probability end, beginning at the 0.1% point. The APDs were only measured to .001% (100 k samples); it is likely that the peak values for the wider bandwidths might have been considerably higher (perhaps 10 dB higher?) had they been extended to the left-hand edge of the graph. The drill APDs are somewhat problematic, since the peak amplitudes of apparently independent pulses do not increase as rapidly as $20 \log_{10} B$. In addition, the very steep slope of the low-probability end makes the measured peak very dependent on the sample size.

Detector summary. The drill detector summary (Figure 8.85) shows that the relative values of the various detectors remain almost the same for all bandwidths; all detectors follow a $10 \log_{10} B$ rule. This behavior fails to match the RF spectrum graphs, which show the peak dB values increasing with a $17 \log_{10} B$ trend line. This discrepancy can be partly explained because the peak measurements for the wider bandwidth spectrum measurements contained a much larger number of independent samples than the narrower bandwidths, which substantially increased the wider bandwidth peak values. It is also likely that the number of "pulses" seen in the drill emission increases proportionately with measurement bandwidth—a much different statistical process than a typical UWB signal (which has a constant number of pulses for wider bandwidths). The Part 15 measurements were too close to system noise to be useful.

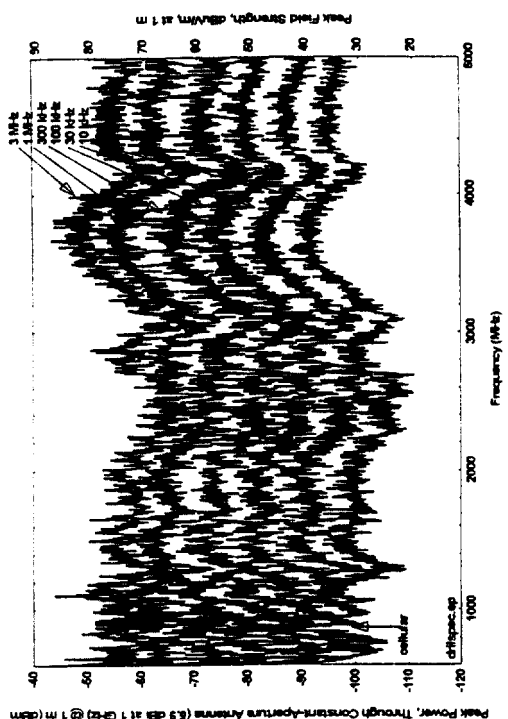


Figure 8.82. Electric drill spectrum as function of measurement bandwidth.

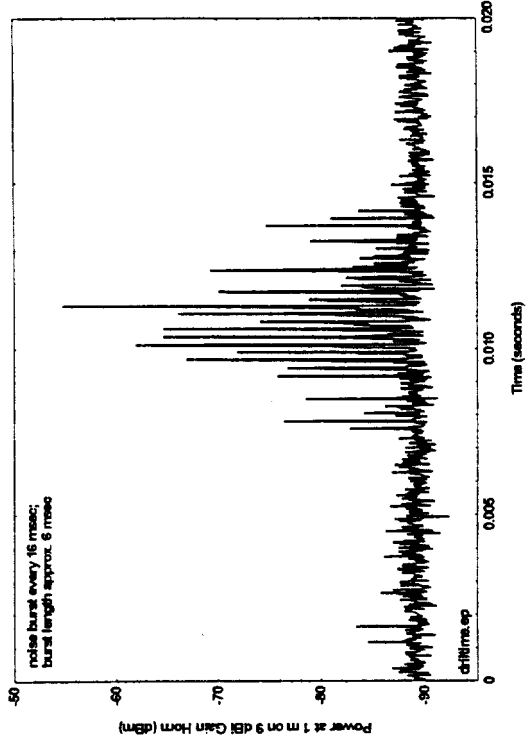


Figure 8.83. Typical electrical drill pulse train.

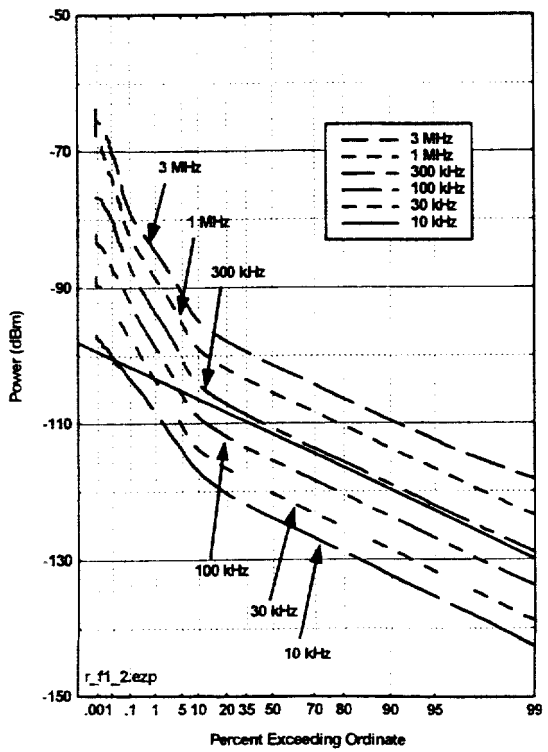


Figure 8.84. Electric drill APDs.

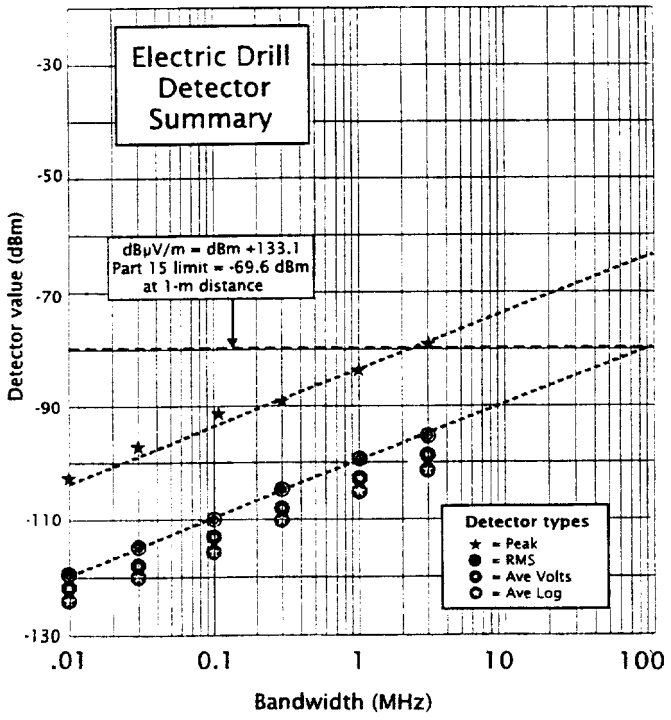


Figure 8.85. Electric drill detector summary.

8.4 Measurement Conclusions

1. The field strength in a bandwidth derived from an FFT of a full bandwidth pulse shape measurement matches the field strength shape measured in a narrower bandwidth by a spectrum analyzer in general shape and absolute amplitude at the peak emission frequency. This confirms that narrowband spectral measurements with a spectrum analyzer or other measurement receiver can be expected to provide accurate information to characterize the overall shape and absolute amplitude of the RF spectrum of UWB signals.
2. Specialized facilities and expertise are needed to obtain accurate measurements of full bandwidth pulse shape. Some of the possible errors associated with this technique are subtle, and many test labs may find that a comparison between FFT-derived spectra and band-limited spectrum analyzer measurements is the only way to verify the accuracy of the full bandwidth pulse shape measurements.
3. There appears to be no simple and accurate technique for relating full bandwidth pulse width data to the 10-dB or 20-dB emission spectra. This is especially true when the UWB pulse is used to excite multiple resonant elements, producing an RF pulse with a multi-lobed ringing response.
4. Amplitude probability distributions (APDs) made with multiple bandwidths provide a useful and theoretically consistent description of UWB signals and how they would affect receivers having various bandwidths. Various detector functions (peak, RMS, average voltage, and average logarithm) can be computed from the APDs or measured directly (if the measurement instrument has the appropriate capabilities).
5. For most UWB devices, the recommended FCC Part 15 non-quasi-peak measurement procedure produces results identical to the average logarithm derived from the 1-MHz bandwidth APD. In situations where the previous statement is not true, the discrepancy is due to insufficient video filtering allowing amplitude variations caused by long-duration duty-cycle events (e.g., gating) to get through to the peak detector.
6. The value measured with an average logarithm detector is substantially affected by measurement system noise for gated or impulsive signals. The average logarithm value is mostly insensitive to energy contained in low-duty-cycle, high-amplitude signals. This results in Part 15 measurement values that can be substantially lower (10-15 dB) than the RMS value (average power) in the UWB signal.
7. The RMS value produces results that are proportional to measurement bandwidth and spectral power density, irrespective of PRR or modulation. Depending on the integration time selected for an RMS measurement, the RMS value can be properly associated with average power when a gated signal is gated on, average power across an entire gating cycle, or average power during other operational periods.

8. Based on measurements of Device C, it seems possible to develop modulation techniques that could cause a UWB signal to look impulsive/gated in a 1-MHz bandwidth and like a CW signal in a 50-MHz bandwidth. Such signals could pass the 1-MHz Part 15 average limit (slipping high-power impulsive signals through the Part 15 average logarithm detector) and the 50-MHz 20-dB peak-to-average limit, while containing average power 15-20 dB above the Part 15 numerical limits. In fact, a signal could probably be designed so that its average power would be within a few dB of the peak level permitted in a 50-MHz bandwidth, while still passing the 1-MHz Part 15 average logarithm limit.

9. A Part 15 average limit based on RMS values would not have the problems described in #6, #7, and #8.

10. Many UWB devices employ dithering, which make their emissions appear more like Gaussian noise (for bandwidths less than the PRR). While this technique is at least partially successful, the specific modulation and dithering techniques may leave a spectrum fine structure that contains many low-level discrete spectral lines and/or other time or frequency distributions that are significantly different from Gaussian behavior. Some of these non-Gaussian characteristics may tend to disappear when actual data are transmitted by UWB devices used for communications, but this effort did not test UWB devices under these conditions.

11. For UWB signals measured with a spectrum analyzer using bandwidths larger than the average PRR, the peak measured values varied according to a $20 \log_{10} B$ rule.

12. Spectrum analyzers having a 50-MHz bandwidth are not yet readily available at test laboratories. A 20-MHz measurement bandwidth was the largest spectrum analyzer bandwidth used in these tests to make peak measurements. Based on #11, a useful alternative to making peak measurements in a 50-MHz bandwidth may be to make measurements in a smaller bandwidth (but large enough that the UWB signal looks impulsive) and to extrapolate to a 50-MHz bandwidth using a $20 \log_{10} B$ rule.

13. We encountered a wide variation of center frequencies (300 MHz to 5 GHz), spectral shapes (very broad to quite narrow), PRR (10 kHz to 10 MHz), modulation techniques (none, absolute dither, relative dither, on-off), gating structures (none, 20%-90%), power levels, and operational functions (short-range to long-range sensing, one-way and two-way communications).

14. Based on measurements of a small sample of existing UWB devices, we are unable to easily or confidently assign UWB devices to a limited number of operational categories having certain distinctive technical characteristics. Therefore, it seems unwise to base any proposed regulations on the assumption that future UWB devices will limit themselves to a few applications and techniques that have been currently developed and demonstrated. Instead, it should be assumed that designers of future UWB devices will creatively explore many additional extensions and combinations of these technologies, and that any UWB device permitted by the regulations will eventually be developed -- possibly in large quantities.

15. Based on measurements of multiple UWB devices, as well as theoretical considerations, the following model (Figure 8.86) describes idealized detector response rules for peak and RMS detectors. This is an idealized treatment, which may or may not apply exactly to specific real systems. One assumption is that the UWB dithering or modulation produces a signal whose narrowband statistics are indistinguishable from Gaussian noise. Actual real-world dithering techniques may or may not approach this ideal, and some UWB devices (e.g., Device C) use dithering techniques whose narrow bandwidth results are quite non-Gaussian. The model assumes that the total number of pulses/s remains equal to the PRR; i.e., that neither gating, on-off keying (OOK), or other dithering/modulation techniques significantly changes the total number of pulses emitted.

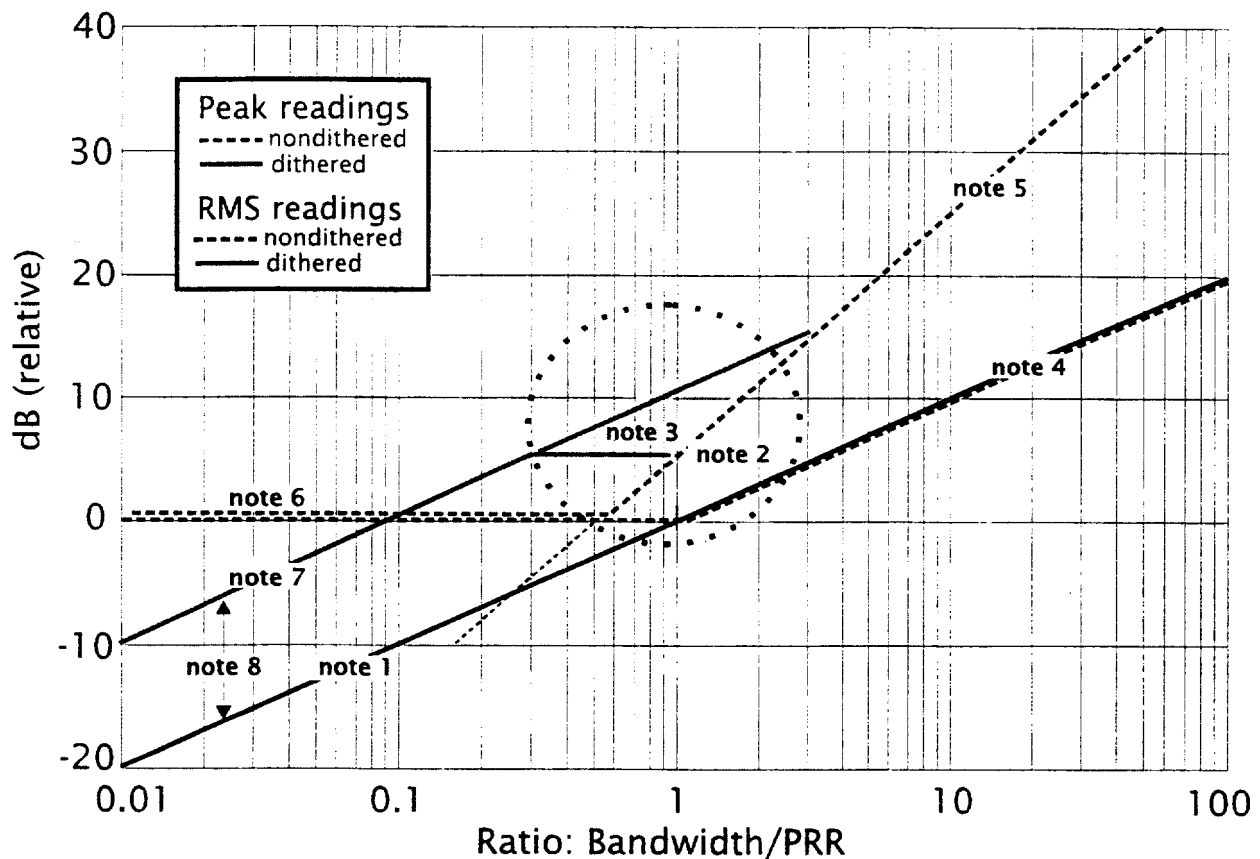


Figure 8.86. Idealized peak and RMS detector values model.

Figure 8.86 describes how a UWB signal measured with peak or RMS detectors in a given a bandwidth can be converted to corresponding readings in another bandwidth. This graph is referenced to the ratio of receiver bandwidth, B , to pulse repetition rate, PRR. This ratio (rather than any particular bandwidth or PRR) is what is critical in determining the rules that govern detector readings. Values of $B/PRR \gg 1$ give non-overlapping impulse responses (the impulsive region). Values of $B/PRR \ll 1$ give overlapping responses that look like Gaussian

noise (dithered case) or discrete CW lines (non-dithered case). Values of $B/PRR = 1$ represent transitional cases, whose behavior varies depending on the details of the modulation on the PRR. The figure shows readings for peak and RMS detectors, for dithered and non-dithered UWB signals. The figure assumes that no gating is present. If gating is present, the figure should be modified by reducing all RMS readings by $10 \log D$, where D is the gating duty cycle, and leaving all peak readings unchanged. The following notes expand on several of the details of the figure.

Note 1. The dithered RMS detector response strictly follows a $10 \log_{10} B$ line, since it is assumed that the total power intercepted by the measurement receiver is strictly proportional to receiver bandwidth. This will be the case for dithered UWB signals for all B/PRR ratios, as well as for B/PRR substantially greater than 1 for the non-dithered case, where the number of discrete CW lines within a bandwidth is proportional to the value of B .

Note 2. The detailed shape of all of these curves near the transition value $B/PRR = 1$ is not well known. It will depend substantially on the details of the UWB device modulation and receiver bandwidth filter response. Filter shapes with sharp suppression of adjacent channel responses will typically have an extended time response and a smaller peak value (i.e., will appear like a smaller bandwidth with respect to the peak value and the duration of the pulse). In general, the slope of the various response curves is trustworthy for bandwidth values far away from the transition point, but neither the exact shape of the transition curves nor the straight-line intercepts between the noise-like and impulse-like regions have been precisely determined for a variety of bandpass characteristics and UWB modulations..

Note 3. The behavior near the transition region where $B/PRR = 1$ for "dithered peak" is particularly obscure. This is partly because there is a transition between a Gaussian probabilistic region and a deterministic impulsive environment. The area in the shaded triangle represents a range of responses that has been observed in this set of measurements, but this region should be examined more carefully. Some measured systems show a very tight grouping of detector readings (4-5 dB difference between average log and peak) when $B/PRR = 1$, while other systems do not.

Note 4. Since impulses have no time overlap in the impulsive region ($B/PRR \gg 1$), there is no difference in responses between dithered and non-dithered pulses. Therefore, the dithered and non-dithered RMS curves will overlay exactly in the $B/PRR \gg 1$ region, and both will follow a $10 \log_{10} B$ slope.

Note 5. For the same reasons described in note 3, the dithered and non-dithered peak curves will overlay exactly in the $B/PRR \gg 1$ region, and both will follow a $20 \log_{10} B$ slope.

Note 6. The response for non-dithered UWB pulses produces evenly-spaced discrete CW lines when $B/PRR \ll 1$. The graph assumes that measurements are made centered on one of the discrete CW lines. Since the envelope response for a single CW line is a constant voltage, the peak and RMS detectors give the same response. Moreover, since the voltage remains constant

for all bandwidths (assuming that the measurement bandpass remains centered on the CW signal), the common response for peak and RMS detectors follows a single horizontal line for $B/PRR \ll 1$.

Note 7. The value of the dithered peak reading will be about 10 dB above the value of the dithered RMS reading. This is based on the assumption that dithering produces statistics identical to Gaussian noise for $B/PRR \ll 1$. Also, see Note 8.

Note 8. It should be noted that the ratio between peak and RMS for detected Gaussian noise is not a constant; instead, it is a statistical quantity that depends on the number of independent observations. For example, there is a 1% chance that the peak will exceed the RMS by about 7 dB, a 0.1% chance of exceeding the RMS by about 8.5 dB, a 0.01% chance of exceeding the RMS by about 10 dB, etc. Therefore, the 10-dB peak-to-RMS ratio is based on collecting the peak reading from 10,000 independent observations. The peak-to-RMS ratio may need to be adjusted to use other probabilities, depending on the exact circumstances of how the model is to be applied.